Computational and Structural Biotechnology Journal 20 (2022) 5622–5638

COMPUTATIONAL ANDSTRUCTURAL BIOTECHNOLOGY JOURNAL

journal homepage: www.elsevier.com/locate/csbj

Integrative analysis of macrophage ribo-Seq and RNA-Seq data define glucocorticoid receptor regulated inflammatory response genes into distinct regulatory classes

Suhail A. Ansari [a,1], Widad Dantoft [a,1], Jorge Ruiz-Orera [c], Afzal P. Syed [a], Susanne Blachut [c], Sebastiaan van Heesch [d], Norbert Hübner [c,e], Nina Henriette Uhlenhaut [a,b,*]

[a] Institute for Diabetes and Endocrinology (IDE), Helmholtz Center Munich (HMGU) and German Center for Diabetes Research (DZD), Neuherberg, Germany
[b] Metabolic Programming, School of Life Sciences Weihenstephan, ZIEL – Institute for Food and Health, Technical University of Munich (TUM), Freising, Germany
[c] Cardiovascular and Metabolic Sciences, Max Delbrück Center for Molecular Medicine in the Helmholtz Association (MDC), Berlin, Germany
[d] Princess Máxima Center for Pediatric Oncology, Heidelberglaan 25, 3584 CS Utrecht, The Netherlands
[e] Charite-Universitätsmedizin Berlin, Berlin, Germany

ARTICLE INFO

Article history:
Received 15 July 2022
Received in revised form 28 September 2022
Accepted 28 September 2022
Available online 3 October 2022

Keywords:
Glucocorticoid receptor
Macrophages
Inflammation
Ribosome profiling
RNA-seq
Translational regulation

ABSTRACT

Glucocorticoids such as dexamethasone (Dex) are widely used to treat both acute and chronic inflammatory conditions. They regulate immune responses by dampening cell-mediated immunity in a glucocorticoid receptor (GR)-dependent manner, by suppressing the expression of pro-inflammatory cytokines and chemokines and by stimulating the expression of anti-inflammatory mediators. Despite its evident clinical benefit, the mechanistic underpinnings of the gene regulatory networks transcriptionally controlled by GR in a context-specific manner remain mysterious. Next generation sequencing methods such mRNA sequencing (RNA-seq) and Ribosome profiling (ribo-seq) provide tools to investigate the transcriptional and post-transcriptional mechanisms that govern gene expression. Here, we integrate matched RNA-seq data with ribo-seq data from human acute monocytic leukemia (THP-1) cells treated with the TLR4 ligand lipopolysaccharide (LPS) and with Dex, to investigate the global transcriptional and translational regulation (translational efficiency, ΔTE) of Dex-responsive genes. We find that the expression of most of the Dex-responsive genes are regulated at both the transcriptional and the post-transcriptional level, with the transcriptional changes intensified on the translational level. Overrepresentation pathway analysis combined with STRING protein network analysis and manual functional exploration, identified these genes to encode immune effectors and immunomodulators that contribute to macrophage-mediated immunity and to the maintenance of macrophage-mediated immune homeostasis. Further research into the translational regulatory network underlying the GR anti-inflammatory response could pave the way for the development of novel immunomodulatory therapeutic regimens with fewer undesirable side effects.

1. Introduction

Gene regulatory networks (GRNs) are continually adjusting mRNA and protein levels according to cellular needs, affecting all steps of the expression process, from transcription to mRNA maturation, transport, translation, and protein degradation [1]. These adjustments are further customized in the presence of external stimuli that transform the transcriptional and translational landscapes within the cells.

Over the last two decades, assessing gene transcription levels using next generation sequencing methods such as RNA-seq, have become central to the understanding of the molecular mechanisms underpinning the biological processes and phenotypes in various biological contexts. RNA-seq analysis can, however, not always capture the full picture of gene expression, as the final fate of mRNA molecules depend on mRNA stability, mRNA degradation, and translation efficiency (TE). ribo-seq offers a quantitative approach to study translational regulation of global transcriptomes by quantifying the capture of ribosome-protected RNA fragments

* Corresponding author.
E-mail addresses: henriette.uhlenhaut@tum.de, henriette.uhlenhaut@helmholtz-muenchen.de (N.H. Uhlenhaut).
[1] Equal contribution.

https://doi.org/10.1016/j.csbj.2022.09.042
2001-0370/

(RPFs) [2]. Normalizing ribosome footprint density by mRNA abundance determines a gene's translation efficiency. In ribo-seq, the number of RPFs between different conditions for a given gene is used as a proxy for a change in the translation of the encoded protein. A major caveat with ribo-seq is, however, the mRNA abundance of the transcript, which directly affects the probability of ribosome occupancy, and thus may not necessarily reflect the transcriptional efficiency of each gene.

Synthetic glucocorticoids (GCs) such as dexamethasone (Dex), are commonly used in the treatment of a variety of immune and inflammatory diseases due to their potent anti-inflammatory effect. Their immunomodulatory properties stem from a complex mechanism of action that dampens cell-mediated immunity by inhibiting the expression of pro-inflammatory cytokines and chemokines, while activating the expression of anti-inflammatory immune mediators [3–6]. The effects of GCs are mediated through the ubiquitously expressed intracellular, ligand-dependent glucocorticoid receptor (GR). GR classically exerts its transcriptional regulation, following GC binding, by interacting with evolutionarily conserved 15 bp palindromic consensus DNA sequences (AGAACANNNTGTTCT) designated as glucocorticoid response elements (GREs). GREs are primarily present in the enhancer and promoter regions of GR target genes and drive, predominantly through protein–protein interactions with co-activators and histone acetyl transferases (HATs), the transcription of anti-inflammatory factors [7–10]. Transcriptional inhibition by GR is, on the other hand, exerted via recruitment of co-repressors such as Glucocorticoid receptor interacting protein 1 (GRIP1) and histone deacetylases (HDACs), disrupting pro-inflammatory NF-κB/interferon response factor3 (IRF3) complexes, and interaction with classical palindromes or with cryptic GREs within NF-κB and AP-1 motifs [11–14] (Fig. S1). Though regulation by GCs/GR has been extensively studied on the transcriptional level, the impact of GCs on post-transcriptional gene regulatory mechanisms is largely unknown, with the exception of a small subset of pro-inflammatory genes. These include effector molecules such as Tumor necrosis factor alpha (TNFα), interleukin 6 (IL6), and Chemokine (C—C motif) ligands (CCL)2 and CCL7, suggesting a role for GCs/GR in post-transcriptional gene expression modulation [15–18].

In the present study, we aimed at systematically investigating the global impact of Dex treatment on the transcriptional and post-transcriptional regulation of gene expression in an inflammatory setting. For this, a well-established *in vitro* model of inflammation using macrophage-like cells derived from phorbol 12-myristate 13-acetate (PMA)-differentiated human THP-1 cells was utilized [19]. THP-1 is a human monocytic cell line derived from a patient with acute monocytic leukemia, which has been widely used to investigate monocyte/macrophage activities [20]. Differentiated THP-1 cells are extremely sensitive to LPS and respond by releasing a plethora of inflammatory cytokines [21–23]. To investigate the effect of Dex on inflammation, Dex treatment was performed concurrently with LPS stimulation, with the latter inducing a pro-inflammatory M1 macrophage phenotype. Further, using previously published methodology and integrating matched mRNA-seq data with ribo-seq data, the change in translation efficiency (ΔTE) was calculated [24]. This approach allows the subcategorization of genes into buffered, forwarded, intensified, or exclusively (exclusive) translationally regulated genes. We show that the expression of the majority of the Dex-responsive (activated and suppressed) and LPS-stimulated genes can be classified as "intensified". These genes undergo statistically significant transcriptional and translational changes and display a change in translational efficiency. Overrepresentation analysis (Reactome pathways, KEGG pathways, and gene ontology (GO)), combined with STRING protein network analysis and gene-by-gene manual functional exploration, identified these genes to exhibit immune effector and immunomodulatory functions that contribute to maintaining macrophage-mediated immune homeostasis.

Overall, our findings show that, in addition to transcriptional control, most Dex-responsive genes are subject to translational regulation in LPS-stimulated macrophages, and that the protein products of these genes are involved in macrophage-mediated immunity.

2. Materials and methods

2.1. Cell propagation, culture, and treatment

THP-1 cells were obtained from ATCC and cultured in RPMI 1640 medium (Thermo Fisher Scientific; A1049101) supplemented with 10 % heat inactivated FBS (Sigma Aldrich; F9665), 1 % Pen/Strep (Sigma Aldrich; P4333). The cells were grown at 37 °C and 5 % CO_2 and routinely tested negative for mycoplasma contamination. For THP-1 differentiation, cells were grown in culture media containing the dialyzed FBS (Sigma Aldrich; F0392) and incubated with 10 ng/ml (final concentration) phorbol 12-myristate 13-acetate (PMA, Sigma Aldrich; P1585) for 24 h, followed by 24 h incubation with fresh growth media (without PMA). The differentiated THP-1 cells were treated for 3 h with vehicle (0.1 % EtOH), 100 ng/ml lipopolysaccharide (LPS, Sigma Aldrich; L6529), or with a combination of 100 ng/ml LPS and 1 μM Dex (Sigma Aldrich; D4902). All treatments were performed on five independent biological replicates (n = 5). Following the 3 h incubation, the cells were harvested for ribosome profiling and mRNA sequencing.

2.2. Ribosome profiling

Ribosome profiling of THP-1 derived macrophage-like cells was performed according to previously published work by our group and others [25–27]. In short, 10 million cells were lysed for 10 min on ice in 1 mL lysis buffer consisting of 20 mM Tris-Cl (pH 7.4), 150 mM NaCl, 5 mM $MgCl_2$, 1 % Triton X-100, 0.1 % NP-40, 1 mM dithiothreitol, 10U/ml DNase I, cycloheximide (0.1 mg/ml) and nuclease-free H_2O. The lysate was homogenized by immediate repeated pipetting and multiple passes through a syringe fitted with a 21G needle, allowing for dissociation of cell clumps and facilitating quick and equal lysis of the cells. Samples were next centrifuged at 20,000g for 10 min at 4 °C to pellet cell debris. Per sample, 200 or 400 μL of lysate were digested with RNase 1 (N6904K; Biozym), purified with Microspin Sephacryl S-400 HR columns (Sigma-Aldrich; GE27-5140–01) and 1μg footprints were used for removal of the ribosomal RNA according to the ribo-Zero Gold rRNA Removal Kit (h/m/r) (Illumina; MRZG12324). The footprints were purified by excision from a Novex 15 % TBE Urea PAGE gel (Fisher Scientific; EC68852BOX) followed by a treatment of the 3ends with T4 PNK (Biozym; P0503K) to allow ligation to a pre-adenylated linker. The RNA was then reverse transcribed with Reverse Transcriptase (Biozym; ERT12925K) and the cDNA purified via a Novex 10 % TBE Urea PAGE gel (Fisher Scientific; EC68752BOX). The fragments were circularized using Circligase I (Biozym; CL4115K) followed by a PCR amplification and size selection using a Novex 8 % TBE PAGE gel (Fisher Scientific; EC62152BOX). For all samples, ribosome profiling library size distributions were checked on the Bioanalyzer 2100 using a high sensitivity DNA assay (Agilent; 5067–4626), multiplexed and sequenced on a NovaSeq 6000 Illumina producing single end 1x51nt reads. The samples were processed in one batch to avoid a sample processing bias. THP-1 macrophage ribo-seq libraries were sequenced to an average depth of 80 M (min. 64 M, max. 91 M) raw reads.

2.3. Stranded mRNA sequencing

Total RNA was isolated using TRIzol Reagent (Invitrogen; 15596018) using 3 million of the exact same human THP-1 derived macrophage-like cells processed for ribosome profiling. RIN scores were measured on a BioAnalyzer 2100 using the RNA 6000 Nano assay (Agilent; 5067–1511). Poly(A)-purified mRNA-seq libraries were generated from high quality RNA (average RNA Integrity Number (RIN)) of 7.7. RNA-seq library preparation was performed according to the TruSeq Stranded mRNA Reference Guide, using 500 ng of total RNA as input. Libraries were multiplexed and sequenced on an Illumina NovaSeq 6000 producing paired 2x101nt reads. THP-1 macrophage mRNA-seq libraries were sequenced to an average depth of 160 M (min. 81 M, max. 207 M) raw reads.

2.4. RNA-seq and ribo-seq data analysis

Ribo-seq and RNA-seq were analyzed as previously described [28]. Before genome mapping, Ribo-seq reads were clipped to remove residual adapters using the FASTX toolkit (https://hannonlab.cshl.edu/fastx_toolkit/). Reads mapping to the ribosomal RNA and tRNA sequences were removed with Bowtie2 v2.4.5 [29]. The paired mRNA-seq reads (2x101nt) were trimmed to 29-mers (the average length of Ribo-seq reads) to reduce any read length or filtering bias towards mapping or quantification. This was done in order to establish the comparability of the data obtained from Ribo-seq and RNA-seq. Ribo-seq and trimmed RNA-seq reads were then mapped to the human reference genome (GRCh38, Ensembl v87) using STAR v2.7.10a [30]. During the alignment step, the following parameters were used: "--limitIObufferSize300000000--limitOutSJcollapsed10000000--outSAMattributesAll--outFilterMultimapNmax20--outFilterMismatchNmax 2 --alignSJoverhangMin 1000--twopassMode Basic".

2.5. Prediction and differential translation of actively translated ORFs

Actively translated ORFs were detected with ORFquant 1.00 [31] using a pooled set including all mapped ribo-seq samples. We only considered ORFs with a minimum number of 15P-sites in: i) cells treated with lipopolysaccharide (LPS), and ii) cells treated with a combination of lipopolysaccharide (LPS) and Dex. Predicted ORFs were divided into six considered sORF biotypes: CDS (annotated coding sequences, partially or totally in-frame), lncRNA ORFs (lncRNA-ORFs, encoded by presumed long non-coding RNAs), ncRNA ORFs (ncRNA-ORF, encoded by processed transcripts of protein-coding genes), upstream ORFs (uORFs, encoded by 5′ UTR sequences), internal ORFs (intORFs, fully overlapping an annotated CDS in an alternative frame), and downstream ORFs (dORFs, encoded by 3′ UTR sequences)).

Next, P-site counts were extracted with RiboseQC (https://doi.org/10.1101/601468). In-frame P-site counts were quantified for each called ORF and used as input to identify differentially translated ORFs with DESeq2 v1.26.0 [32]. ORFs with an absolute fold change equal or higher than 1.5 and an adjusted p-value lower than 0.01 were defined as differentially translated.

2.6. Quality control (QC) analysis of ribo-seq data

An algorithm called ribo-TIS Hunter (ribo-TISH) was used to perform quality control analysis on the mapped RPFs [33]. RPFs distribution around annotated coding genes and grouping by read length were checked using the "quality" function of this toolkit. RPF 5′ end distribution near annotated gene start codons is assessed for each read group before estimating P-site offsets. The RPF count between the 15 bp upstream of the first base of the start codon and the 12 bp upstream of the first base of the stop codon was taken into account when calculating the RPF count distribution in three reading frames as well as the CDS metagene profile. The ratio between the highest RPF count across all three reading frames and the total of all RPF counts was used to calculate the percentage of RPF counts in the dominant frame. Furthermore, RPF counts between −40 and +20 bp of the start/stop codon's first base were summed across all annotated genes to generate an RPF count profile near the start/stop codon.

Further QC analysis was performed using the RiboWaltz R package to identify P-sites and calculate the distance of the P-site from the start and stop codons of the coding sequence. Furthermore, the tool returns the data structure used to calculate the distribution of P-site across transcript regions (5′ UTR, CDS, and 3′ UTR) and trinucleotide (3-nt) periodicity covered by the P-site [34].

2.7. Identification of translationally regulated genes

The quantification of gene expression was accomplished by using featureCounts v2.0.1 to count the number of reads that mapped to a known genomic and transcriptomic reference [35]. DESeq2 v1.26.0 statistical model (design=∼Condition + SeqType + Condition:SeqType) was used to normalize gene counts with respect to size factor or other normalization parameters for both ribo-seq and RNA-seq data [32]. The translation efficiency of genes was calculated by combining RPF and mRNA counts, and then the deltaTE (ΔTE) method in R was used to identify genes that were differentially and translationally regulated, as described by Chothani *et. al.* [20]. A false discovery rate (FDR) threshold value of 0.05 was utilized as a cutoff to quantify change in translation efficiency for each gene and categorize genes into various regulatory classes utilizing the ΔTE approach.

2.8. Pathway enrichment and regulatory network analysis

The gene list from each regulatory class was analysed using the Enrichr R package to test the probability that annotated gene sets were statistically enriched for Gene Ontology (GO) terms (version 2015) based on their participation in biological processes [36]. Associations were considered statistically significant if their adjusted p-values for multiple testing were less than 0.05.

We further performed integrative pathway enrichment analysis on RNA-seq, ribo-seq, and ΔTE datasets using ActivePathways R package with the default parameters [37]. We provided the p-values of differential changes in mRNA, ribosome footprints (RPF), and translation efficiency (TE) of genes listed in each regulatory class as the first input in this three-step method. As a second input, we used gene sets corresponding to the Reactome Databases Molecular Pathways [38] and Gene Ontology Biological Process [39] downloaded from the g:Profiler web server [40]. Specifically, in the first step of the ActivePathways method, adjusted p-values from different datasets for each gene were merged using a statistical data fusion approach, resulting in an integrated gene list [41]. The integrated gene list was then ranked in decreasing order of significance and filtered using the default threshold (unadjusted $p < 0.1$). Step two involved statistical enrichments of pathways using the ranked hypergeometric test, which determines the pathways significantly enriched in the integrated gene list. Step three generated separate gene lists from individual input datasets and performed similar pathway enrichments (as in step 2) with the ranked hypergeometric test, to find supporting evidence for each pathway from the integrative analysis.

To identify key RNA-binding proteins (RBPs) that were differentially expressed in the most prominent "intensified" regulatory class in our data, we used experimental evidence-based databases of RBP-RNA bindings derived from ENCODE [41] and POSTAR3 [42].

To build the RBP - targets regulatory network, the R packages GENIE3 [43], igraph [44], and RCy3 [45] were used. As input data files, log transformed adjusted p-values for genes that were differentially transcribed (DTG) and translationally efficient (DTEG) from a specific biological process (derived from Enrichr analysis) were used. Cytoscape was employed to visualize the RBP-target network [45].

2.9. Expression analysis

Differential expression analysis of genes within each regulatory class was performed using Volcano plots in RStudio (RStudio Team (2022)). RStudio: Integrated Development Environment for R. RStudio, PBC, Boston, MA URL https://www.rstudio.com/.) using the ggplot2 package (Wickham H (2016). *ggplot2: Elegant Graphics for Data Analysis*. Springer-Verlag New York. ISBN 978-3-319-24277-4, https://ggplot2.tidyverse.org). Lists of significant and non-significant DEGs are compiled in Supplementary file 1. Comparative gene analysis using Venn diagrams of significantly up ($log2FC \geq 0.58$, p adj ≤ 0.05) and downregulated ($log2FC \leq -0.58$, p adj ≤ 0.05) differentially expressed genes (DEGs) was done using the online software tool VENN DIAGRAMS generated by the Van de Peer Lab (https://bioinformatics.psb.ugent.be/webtools/Venn/). Comparisons were done between genes categorized as "intensified" within each platform (RNA-seq and ribo-seq). Output control parameters were set to Non-symmetrical Venn Diagram Shape and Colored Venn Diagram Fill.

2.10. Enrichment and STRING network analysis

Enrichment analysis was done on significantly up ($log2FC \geq 0.5849625$, p adj ≤ 0.05) and downregulated ($log2FC \leq -0.5849625$, p adj ≤ 0.05) differentially expressed genes (DEGs) (LPS + Dex vs LPS) identified in the RNA-seq dataset. Over-Representation Analysis (ORA) of Reactome Pathways was done using the WEB-based Gene SeT AnaLysis Toolkit (WebGestalt, https://www.webgestalt.org) [46]. Analysis was done using ensemble gene IDs as input data, "genome" as Selected Reference Set, and the default advanced parameters provided by the website (statistical significance (FDR ≤ 0.05) was calculated using Benjamini-Hochberg Procedure). Plots of the Top 10 ORA Reactome Pathways were generated in RStudio (RStudio Team (2022). RStudio: Integrated Development Environment for R. RStudio, PBC, Boston, MA URL https://www.rstudio.com/.) using the ggplot2 package (Wickham H (2016). *ggplot2: Elegant Graphics for Data Analysis*. Springer-Verlag New York. ISBN 978–3-319–24277-4, https://ggplot2.tidyverse.org.). STRING network analysis was performed in Cytoscape 3.9.1 [47] using the Cytoscape stringAPP [48] (medium confidence cutoff, 0.400). To group the proteins in the network based on their interactions from STRING, clusterMaker2 [49] was used to run Markov clustering (MCL) [50]. The MCL granularity parameter (inflation value) was set to 4 and array source was set to use the STRING confidence score attribute (stringdb::score) as weights. All other settings were kept at default. Functional enrichment analysis was performed on the top four subnetworks (clusters 1–4) using the stringAPP with an FDR threshold of 5 % (FDR ≤ 0.05), generating lists of terms spanning 14 categories: GO Biological Process, GO Molecular Function, GO Cellular Component, DISEASE, KEGG Pathways, Reactome Pathways, and WikiPathways. Functional enrichment analysis of the networks from the upregulated "intensified" DEGs resulted in 399 statistically significant terms, and analysis of the networks from the downregulated "intensified" DEGs resulted in 1167 statistically significant terms. Each list of terms was filtered to eliminate redundant terms (using the default redundancy cutoff of 0.5), resulting in reduced lists of 108 enriched terms for the networks from the upregulated "intensified" DEGs and 369 enriched terms for the networks from the downregulated "intensified" DEGs. Enrichment analysis of STRING network clusters of "buffered" DEGs identified 44 enriched terms before filtering and 9 enriched terms after filtering, enrichment analysis of "exclusive" DEGs identified 163 terms before filtering and 24 after filtering. Of these, the four most significant terms (FDR ≤ 0.05) from each analysis were chosen.

2.11. Statistical analysis

For differential expression analysis with DESeq, the Wald test was used when comparing the two treatment conditions. In addition, a deltaTE equivalent interaction coefficient that is equal to translation change and independent of transcriptional change was introduced into the DESeq statistical model [24]. In ActivePathways, Brown's extension of the Fisher's combined probability test was utilized to generate merged p-values from multiple datasets. The regulatory link generated by GENIE3 was ranked by a random forest algorithm [43].

3. Results

3.1. Quality control analysis of ribo-seq data

The human monocyte cell line THP-1 was utilized to examine the overall effects of the synthetic glucocorticoid Dexamethasone (Dex) on the transcriptional and post-transcriptional regulation of gene expression in the context of macrophage innate immunity. Phorbol 12-myristate 13-acetate (PMA) was used to differentiate THP-1 cells into macrophages (henceforth referred to as macrophages), and then LPS stimulation was used to establish a pro-inflammatory M1 macrophage phenotype. The modulatory effect of Dex on LPS induced macrophages was analyzed using an integrated approach combining the mRNA sequencing and Ribosome profiling (Fig. 1A). In general, ribo-seq data provides a global snapshot of all the translating ribosomes and predicts the protein abundance in a population of cells at a given time.

At the core of ribo-seq experiments is the formation of mRNA-ribonucleoprotein complexes by translating ribosomes. These mRNA-ribonucleoprotein complexes are resistant to digestion by nucleases and serve as ribosome-protected footprints (RPFs) in a sequencing scenario. Thus, the sequencing of these RPFs provide precise location of active ribosomes on the translated transcripts (Fig. 1A). Using the sequenced RPFs that were mapped to the annotated coding genes, we identified the translation activities of ribosomes in vehicle treated, LPS stimulated, and LPS + Dex treated macrophages, using a comprehensive statistical toolkit for ribosome profiling, named ribo-TISH [33]. It provides a summary of the distribution of RPF lengths and a measurement of the quality of the size selection. Under all treatment conditions (vehicle control, LPS and LPS + Dex) in our ribo-seq experiment, the size of RPFs, recovered from mapped sequencing data, was typically around 28 nucleotides (nts) (Fig. 1B-D).

Ribo-TISH also provides several QC metrics/profiles based on the RPF length distribution, to evaluate the quality of RPFs of different lengths. The first category of our Ribo-seq data QC profile was the distribution of RPF counts across three reading frames and the fraction of RPF counts (f_d) in the dominant frame within the annotated coding genes at various RPF lengths (Fig. 1B-D). The best quality data was observed for 28 nts RPF length under all treatment conditions, with a higher fraction of RPF counts ($f_d > 0.9$) in the dominant reading frame. Different-length RPFs may have varying data quality (smaller f_d for the RPFs with 26 or 27 nts). A higher RPF count in the data's dominant RPF length also ensures a significant 3-nt periodicity for downstream analysis. Notably, 3-nt peri-

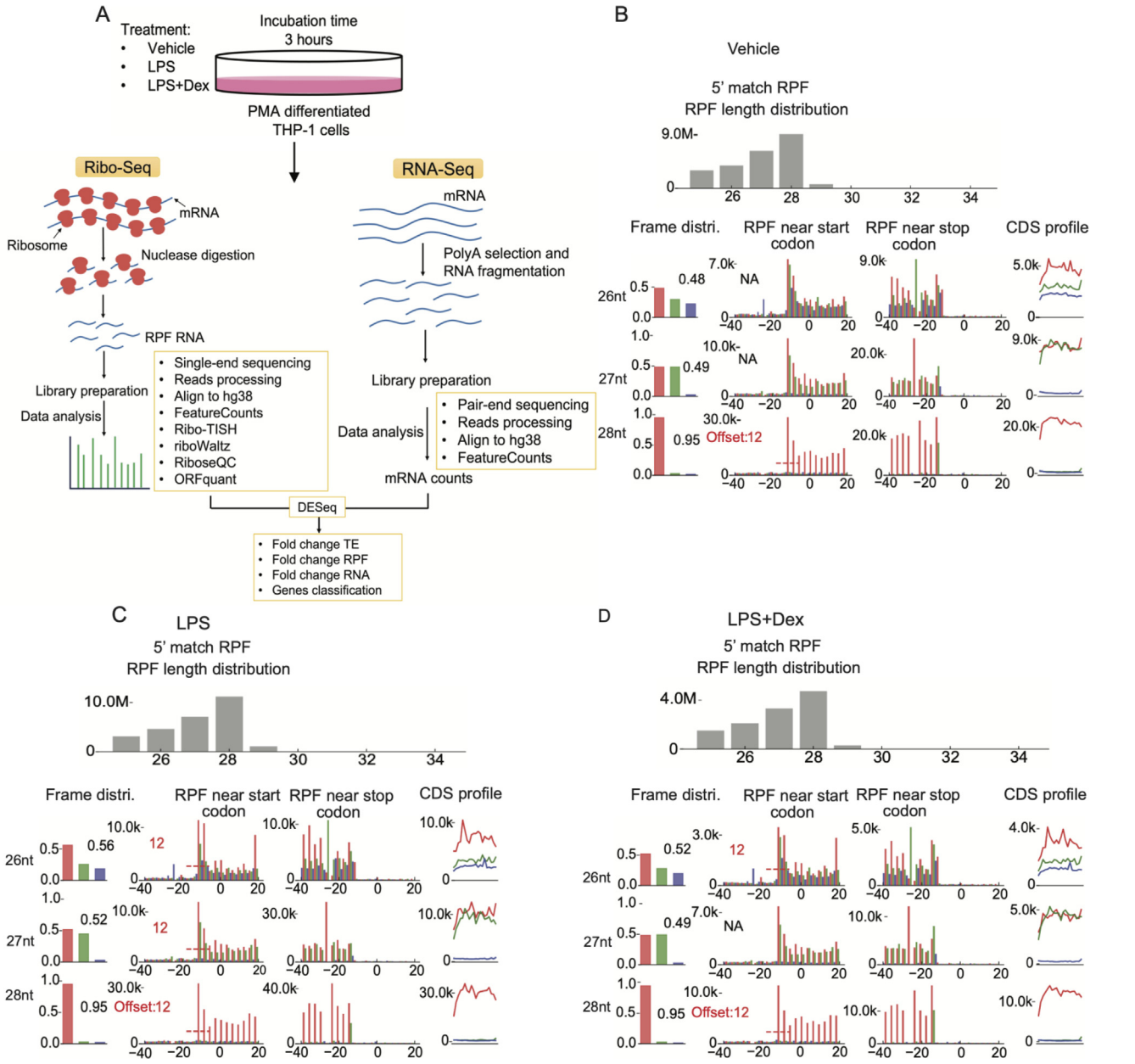

Fig. 1. Experiment summary, computational analysis, and subsequent quality check of ribo-seq data (A) Overview of the ribosome profiling experimental workflow and data analysis. The processed data include five biological replicates for each treatment condition for ribo-seq and four biological replicates for each treatment condition for RNA-seq. (B-D) ribo-TISH analysis for quality control of ribo-seq data of PMA-differentiated THP-1 derived macrophage-like cells treated with control vehicle, LPS, or a combination of LPS and dexamethasone (LPS + Dex). Upper panel: RPF length distribution mapped to annotated protein-coding regions. Lower panel: Different quality profiles/metrics for annotated RPFs. The data for first, second, and third reading frame is represented by the colors red, green, and blue, respectively. Each row displays RPFs with their corresponding lengths. Column 1: Distribution of RPF 5′ ends across all codons and three reading frames, indicating the proportion of RPF counts from the dominant reading frame. Column 2: RPF 5′ end count distribution near annotated TISs. P-site offset and the ratio between RPF counts at annotated TISs and sum of RPF counts near the annotated translation initiation sites (TISs) after correction for P-site offset are shown. Column 3: RPF 5′ end count distribution in close proximity to annotated stop codon. Column 4: RPF count distribution across three reading frames in protein-coding regions (CDS). (For interpretation of the references to color in this figure legend, the reader is referred to the web version of this article.)

odicity is a characteristic primary structure of coding regions in all known organisms [51]. This structural feature is often utilized during bioinformatics analyses to predict the coding sequence and to identify the potential shift in reading frame of a gene [52].

The meta-gene profile of the RPF count near the annotated translation initiation (TIS) and termination sites was shown in the second category of the QC profile (Fig. 1B-D). As expected, in all treatment conditions, our data showed RFP counts increase near the annotated TIS and decrease near the termination site. ribo-TISH computes the distance between the P-site and the 5′ end of the sequenced RPFs (i.e., the P-site offset) based on the meta-gene profile of the 5′ end of the sequenced RPFs in relation to the annotated TIS. The P-site (called peptidyl site) of ribosome binds tRNA holding the growing polypeptide chain [53]. Identifying the P-site position on RPF using ribo-seq data is a critical step in quantitatively analysing translation events at the codon level [54]. The canonical initiating Met-tRNA is base-paired with the AUG start codon at the P-site, which is typically internal to the sequenced RPFs and which serves as the entry point for the first aminoacyl tRNA. For RPFs of varying lengths, the P-site offset can also vary. In our datasets, P-

site offset was found to be 12 nts for the RPFs with a length of 28 nts in all the samples. The P-site offset, on the other hand, varied for RPFs of different lengths (24 and 26 nts). Since a default P-site offset of 12 nts was applied to all reads during the quality control analysis, no value was returned for RPF lengths of 24 nts (vehicle) and 27 nts (vehicle and LPS + Dex treatments). This indicated that RPF maintains a distinct P-site offset of varying length under various treatment conditions.

A third category of QC profile shown is the meta-gene profile of the RPF count across the whole CDS of the annotated protein coding genes. These data show the enrichment of RPF counts at the annotated TIS versus the whole CDS region after P-site offset correction (Fig. 1B-D). In addition, different length RPFs had different meta-gene profiles and RPF enrichment scores at the TIS. Thus, ribo-TISH analysis confirmed various aspects of the quality of our ribo-seq data from the different treatment conditions.

3.2. Genome-wide translational analysis

To further determine the P-sites within ribosome protected fragments at nucleotide resolution, we used the RiboWaltz R package to maximize offset coherence and to improve the interpretation of P-site positional information from the ribo-seq data. This approach provides a meta-gene read density heatmap for every read length, accounting for both the 5′and 3′ ends of the reads. It provides an overview of the occupancy profiles used to determine P-sites and permits visual verification of the accuracy of P-site offset values. Considering that the distance between 5′ ends and TIS is essentially constant for different RPF lengths, a stable 5′ end is the optimal extremity in our ribo-seq data (Fig. 2A). Identifying the ribosome P-site in each RPF is crucial for determining the 3-nt periodicity of translating ribosomes and drawing correct conclusions about ribosome positions. In our ribo-seq data (using a LPS + Dex treated sample as reference), the percentage of P-sites located in the 5′ UTR, CDS, and 3′ UTR regions of mRNAs varied with region length. Expectedly, the CDS of transcripts was emerged as the region with the highest percentage of reads, as well as the highest proportion of P-site enrichment (Fig. 2B). Furthermore, we observed codon periodicity uniquely in the coding sequence (CDS), with no signal along UTRs, neither near start nor stop codons (Fig. 2C). This suggests that the ribosomes were often in a non-translational state outside of the CDS. For each read group, we showed the percentage of P-sites in the three possible translation reading frames (periodicity analysis) for the 5′ UTR, CDS and 3′ UTR in order to determine the extent to which the obtained P-sites lead to codon periodicity in the CDS. The data clearly suggested a P-site enrichment in the first frame of the CDS coding sequence (Fig. 2D-E). To further determine which codons exhibited greater or lesser ribosome density in our data, we analyzed codon usage, i.e. the frequency of in-frame P-sites along the coding sequence (codon by codon), normalized for the frequency of each codon in the sequences. The resulting codon usage indexes highlighted start and stop codons and also detected the frequency of different codons of amino acids used in all translating ORFs in our ribosome profiling data (Fig. 2F).

Next, we identified actively translated ORFs in our macrophages. We categorized these ORFs based on host gene annotation and genomic position relative to known coding regions. As a result, we found a total of 14,967 translated ORFs in both coding and non-coding transcripts, across a wide range of expression values. The vast majority of ORFs (14,266; ∼95 %) were found in protein-coding genes mapped over previously discovered CDS coding domains (Fig. 2G, Fig. S2). Additionally, we identified 416 genes with 462 translated upstream open reading frames (uORF), 10 genes with 11 internal open reading frames (intORF), and 20 genes with 21 downstream open reading frames (dORF) (Fig. 2G, Fig. S2). We also found 207 ORFs encoded by non-coding transcripts in our data, which mainly belonged to the processed transcripts of protein-coding genes (ncRNA) and long noncoding RNA (lincRNA-ORF) biotypes (Fig. 2H, Fig. S2).

3.3. Translational regulation of glucocorticoid receptor target genes in human macrophages

Ribosome profiling also offer a quantitative way to investigate translational regulation by post-transcriptional processes that affect protein levels, including protein stability, protein degradation, and others [55–58]. We applied a deltaTE approach that uses the DESeq2 statistical model to determine the significant changes in interaction term (or ΔTE) under different treatments [24]. The principle component analysis (PCA) was conducted on both ribo-seq and RNA-seq results to determine the source variation in the data other than the treatment. It demonstrated that PC1 explained 74 % of the variance in the RNA-seq (Fig. 3A) and 64 % of the variance in the ribo-seq (Fig. 3B), indicating that sample treatment differences accounted for the major variance in these data. Integrating the RNA-seq and ribo-seq allow the calculation of the change in translation efficiency (ΔTE) of differentially expressed genes, which is the ratio of RPFs over mRNA counts within a gene's coding sequence. The genes were considered translationally regulated that exhibited change in translation efficiency under LPS + Dex condition in macrophages. These genes were also referred to as differential translation efficiency genes or DTEGs. A gene was designated as DTEG specifically if variations in mRNA read counts cannot account for changes in the number of RPFs (Fig. 3C, Supplementary file 1). On the other hand, a differentially transcribed gene (DTG)] is a gene that is transcriptionally but not translationally regulated. These genes showed significant change in mRNA counts as well as RPFs (Fig. 3C, Supplementary file 1).

Taking DTEGs and DTG genes into account, we further combined the changes in RPF, mRNA, and translation efficiency (TE) to determine a gene's regulatory class. A threshold of p adj < 0.05 was used to identify genes that have undergone significant changes in LPS + Dex treatment compared to LPS. The genes were categorized into (i) **Forwarded**: Genes classified as "forwarded" are transcriptionally regulated. There was no change in TE in these genes, and the change in mRNA is responsible for the change in RPFs. Therefore, genes that had significant RPF and mRNA but not significant TE belong to this category. This class contains a total of 55 genes identified as DTG (Fig. 3D, Supplementary file 1). (ii) **Exclusive**: The change in TE is solely driven by the change in RPFs, while mRNA counts remain unchanged. Therefore, this group consists of genes with significant TE and RPFs but no significant change in mRNA counts. Consequently, these genes are only regulated translationally. There is a total of 464 DTEG genes in this class (Fig. 3E, Supplementary file 1). (iii) **Intensified:** These are the genes that are regulated by both transcription and translation (significant change in mRNA, RPFs, and TE). Both DTGs and DTEGs describe these genes. In this case, mRNA changes act with the change in TE. This class contains a total of 1851 genes (Fig. 3F, Supplementary file 1). (iv) **Buffered**: These represent the genes where the transcriptional change is nullified by the change in TE to the extent that RPFs do not change significantly. Consequently, genes with a significant TE and RNA but not a significant RPF are considered to be translationally buffered. This category includes a total of 356 genes (Fig. 3G, Supplementary file 1).

Furthermore, to understand the system-level relationship of transcriptional and translational overlaps, we performed integrative analysis using the ActivePathways method that utilized a statistical fusion approach to discover systematically enriched pathways by combining adjusted p-values from DTG, DTEG and ΔTE data. For the most prominent "intensified" regulatory class,

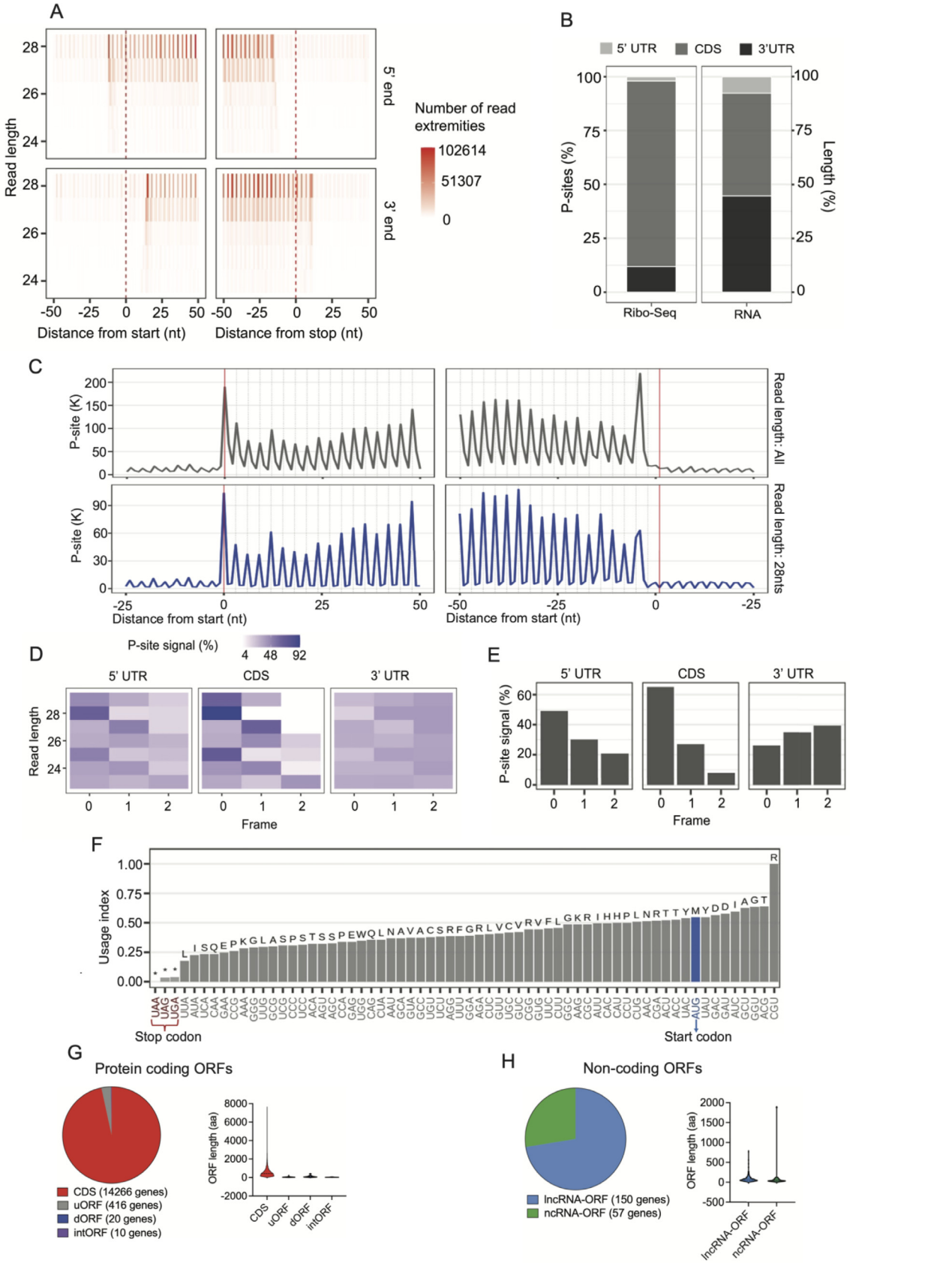

Fig. 2. Ribosome positioning and P-site estimation along mRNAs in LPS and Dex-treated samples. (A) meta-gene heatmaps for various read lengths show the signal at the 5′ end (upper panel) and 3′ end (lower panel) of reads aligned around the start and stop codons. (B) Data from ribosome profiling that shows the percentage of P-sites in the 5′ UTR, CDS, and 3′ UTR of mRNAs (left). Percentage of mRNA sequence region lengths (right). (C) meta-profiles at the genome-wide level displaying the periodicity of ribosomes along the transcripts for all detected read lengths (upper panel) and for reads of 28 nts (lower panel). (D) Read length-based stratification of the percentage of P-sites in the three frames along the 5′ UTR, CDS, and 3′ UTR. (E) P-site enrichment along the 5′ UTR, CDS, and 3′ UTR (all reads combined). (F) Analysis of codon usage: The codon usage index is the frequency of in-frame P-sites along each codon's coding sequence, normalized for codon frequency. Above each bar are the amino acids that match the codons. (G-H) Biotype distribution of all the translated ORFs (protein coding and non-coding ORFs) and ORF length (protein length) coverage in ribo-seq data from macrophages.

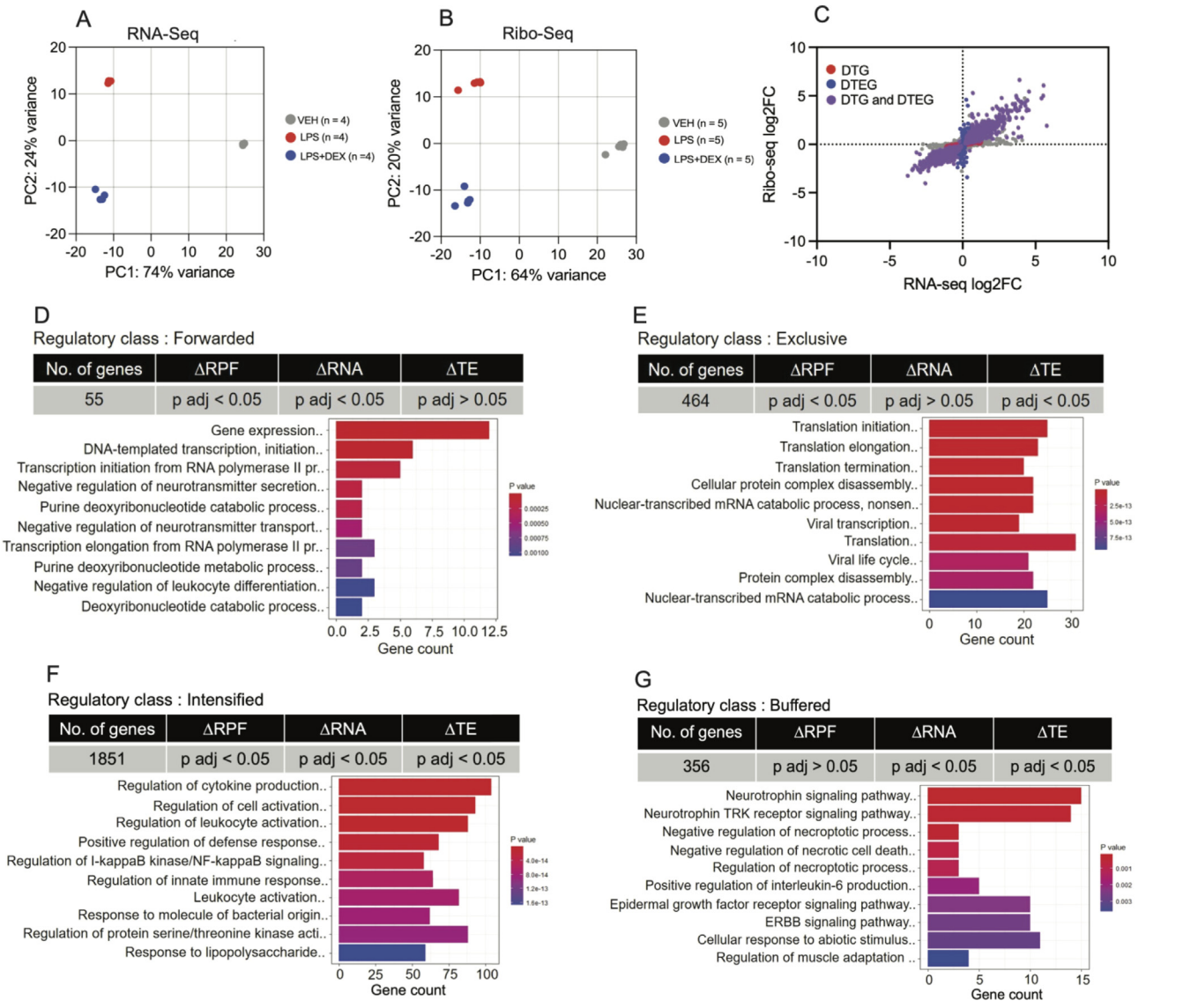

Fig. 3. Genome-wide transcriptional and translational regulation in macrophages by GR. Analysis of the principal components of (A) ribo-seq and (B) RNA-seq datasets from macrophages treated with LPS and Dex. (C) The log fold change values for each gene in the RNA-seq and ribo-seq data are shown in a scatter plot. The genes with differential transcription (DTGs) and translation efficiency (DTEGs) are displayed. (D-G) Profiles of genes and pathways in each regulatory class: forwarded (D), exclusive (E), intensified (F), and buffered (G).

we identified 47 Reactome pathways, where an increase in transcription was also pronounced at the translational level (Fig. S3, Supplementary file 2). 42 Reactome pathways were exclusively regulated at the translational level (Fig. S4, Supplementary file 2). Additionally, ActivePathways identified 15 statistically enriched GO biological processes in translationally buffered DTG, where change in RNA levels of genes were more pronounced than their translation efficiency (Fig. S5, Supplementary file 2) (In this combined p-value based analysis, we were unable to detect enrichment of neither Reactome pathways nor biological processes in the "forwarded" class). Taken together, our analysis showed distinct classes of genes differentially expressed upon GR ligand treatment in inflammatory macrophages, with most GR target genes falling into the "intensified" category. These genes were controlled both transcriptionally and translationally.

3.4. The majority of dexamethasone regulated genes are intensified

The results described above prompted us to investigate the number of highly expressed and significant differentially expressed genes (DEGs) with a FC $\geq$ 1.5 (log2FC $\geq$ 0.58) or below FC $\leq$ -1.5 (log2FC $\leq$ -0.58) (Fig. 4). For identifying possible differences at the transcriptional and translational level, the expression was investigated in the RNA-seq and ribo-seq data separately. Amongst the "forwarded" regulated genes (RNA-seq), the majority of the significant DEGs were found to be suppressed (15 downregulated genes vs 4 upregulated) (Fig. 4A, Supplementary file 3). Similarly, amongst the number of "buffered" genes, 92 genes were found to be downregulated (FC $\leq$ -1.5) while 44 were found to be upregulated (FC $\geq$ 1.5). Interestingly, the number of upregulated (606 genes) and downregulated genes (624 genes) categorized as "intensified" was almost equal. Notably, none of the genes categorized as "exclusive" passed the set log2FC and p adj ($\leq$0.05) cutoffs, suggesting that these genes are exclusively post-transcriptionally regulated.

In the ribo-seq data, none of the genes categorized as "forwarded" regulated were significantly differentially regulated on the translational level (Fig. 4B, Supplementary file 1). Contrary to the RNA-seq data, but consistent with the definition of "exclusively" translationally regulated genes, 103 genes and 58 genes

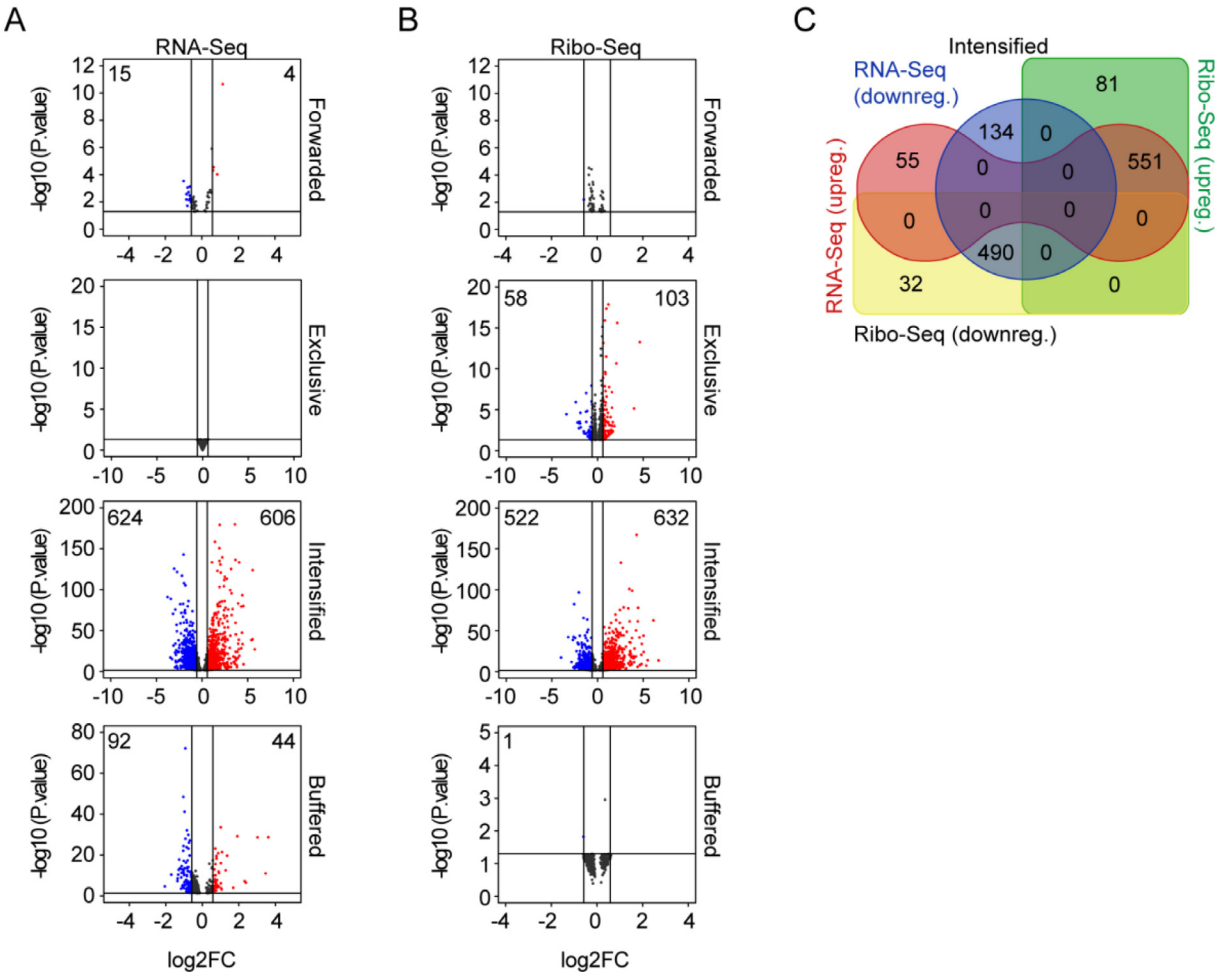

Fig. 4. Majority of dexamethasone regulated differentially expressed genes in LPS-stimulated THP1 cells are under intensified regulation. (A) Volcano plots of up- (red, log2FC ≥ 0.58, p adj ≤ 0.05) and downregulated genes (blue, log2FC ≤ 0.58, p adj ≤ 0.05) identified within each regulatory class in the RNA-seq dataset. (B) Volcano plots of up- (red, log2FC ≥ 0.58, p adj ≤ 0.05) and downregulated genes (blue, log2FC ≤ 0.58, p adj ≤ 0.05) identified within each regulatory class in the ribo-seq dataset. (C) Overlap (Venn diagram) of significantly up- and downregulated "intensified" genes in the RNA-seq and ribo-seq datasets. (For interpretation of the references to color in this figure legend, the reader is referred to the web version of this article.)

were identified as significantly up- and downregulated, respectively. Consistent with the RNA-seq data, the majority of the genes were categorized as "intensified", with exception for one single gene amongst those downregulated (Fig. 4A-B). This additional lone gene (Cardiomyopathy associate 5, *CMYA5*, log2FC = -0.865) was subsequently identified as significantly suppressed in the "buffered" class (Fig. 4A-B). Further comparing the technologies for the number of "intensified" up- and downregulated genes, we identified differences between the RNA-seq and ribo-seq datasets. The increased number of upregulated genes and the decreased number of downregulated genes in the ribo-seq data, together with the observation that these genes exhibited a significant change in ΔTE, suggest that the transcriptional expression of these genes may be further regulated on the translational level.

The observation that the number of "intensified" genes were the different between the RNA-seq and ribo-seq platforms, prompted us to investigate their overlap (Fig. 4C). For this purpose, the DEGs from the volcano plots, identified as up (FC ≥ 1.5, p adj ≤ 0.05) and downregulated (FC ≤ -1.5, p adj ≤ 0.05) were examined. Comparative analysis of the RNA-seq and ribo-seq data with a focus on the significant "intensified" DEGs (up and downregulated genes), identified overlapping and non-overlapping genes (Fig. 4C). 551 genes were found to be commonly upregulated in both profiles (RNA-seq and ribo-seq) and 490 genes were found to be commonly downregulated in both. 81 genes were exclusively found amongst the significantly upregulated, and 32 genes were exclusive for the significantly downregulated DEGs in the ribo-seq data. Simultaneously, in the RNA-seq data, 55 genes were exclusively found in the significantly upregulated, and 134 DEGs were in the significantly downregulated DEGs. As the genes lists were based on the significant DEGs identified in the volcano plots, a closer gene-by-gene analysis of the FC expression values and the adj. p-values (p adj), was done to determine the cause for the presence of non-overlapping genes over the two methodologies. A common denominator for the lack of representation on the opposing data set (ribo-seq for RNA-seq, and vice versa) was the FC expression. That is, the 55 upregulated genes exclusive for the RNA-seq data set had, in the ribo-seq data, a fold change expression below the set cutoff (FC ≥ 1.5). Similarly, the 134 downregulated genes exclusive for the RNA-seq dataset had, in the ribo-seq data, a fold change expression above the set cutoff (FC ≤ -1.5). Conversely, the 81 upregulated genes exclusive for the ribo-seq dataset had, in the RNA-seq data, a fold change expression below the set cutoff (FC ≥ 1.5) and the 32 downregulated genes exclusive for the ribo-seq dataset had, in the RNA-seq data, a fold change expression above the set cutoff (FC ≤ -1.5). Notably, assessing the combined effects of mRNA expression, RPF, and TE demonstrated that well-known GR targets were either "intensified"

upregulated (e.g. *FKBP5*, *KLF4*, *TSC22D3*, *NOS2*, *FOXO1*, *PER1*, *DUSP1* and *SLCO2A1*) or "intensified" downregulated (e.g. *IL1A*, *TNFSF10*, *IL12B*, *CCR7*, *ATF3*, *IL6*, *CXCL9*, *CCL2*) (Fig. S6). Closer inspection identified the those that were "intensified" upregulated (e.g. *FKBP5, KLF4, TSC22D3, NOS2, FOXO1, DUSP1*) as immune-suppressive while in the "intensified" downregulated category chiefly pro-inflammatory molecules (e.g. *IL1A*, *IL6*, *CCR7*) were identified (Fig. S6). Together, these results suggest that for the majority of the Dex-responsive DEGs, the transcriptional change was "intensified" by a translational change in the same regulatory direction (activation/suppression).

3.5. The expression of LPS and dexamethasone responsive immune-regulatory genes are under intensified regulation

With most of the Dex-responsive DEGs being categorized as "intensified", we next proceeded to explore the biological function of the genes in this category (Fig. 5). For this purpose, we focused our analysis on the RNA-seq dataset and the significant DEGs from the volcano plots, identified as up- (FC $\geq$ 1.5, p adj $\leq$ 0.05) and down-regulated (FC $\leq$ -1.5, p adj $\leq$ 0.05) were examined. Overrepresentation analysis (ORA) of the upregulated DEGs identified a significant enrichment for Reactome Pathway categories associated with downstream intracellular signaling events (e.g., Semaphorin interactions, Interleukin-17 signaling, Response to metal ions, and MAP kinase activation) (Fig. 5A). While pathways associated with pattern recognition (e.g., Toll-like Receptor TLR6:TLR2 Cascade, Toll-like Receptor TLR1:TLR2 Cascade, G alpha (q) signaling events, and MyD88:MAL (TIRAP) cascade initiated on plasma membrane) were identified amongst the top 10 pathways, their enrichment was non-significant (FDR $\geq$ 0.05) (Fig. 5A). These enrichment results were further underpinned by protein network analysis using the Cytoscape software [47]. STRING protein network analysis was done using the Cytoscape stringAPP [48] with subsequent Markov clustering (MCL) and functional enrichment analysis of the top four clustered subnetworks (clusters 1–4). Network analysis and manual analysis of gene function identified the top four subnetworks as 'inflammatory related' (Fig. 5B). In addition to Interleukin (IL)15, IL27 receptor alpha (IL27RA), and the interferon lamda receptor 1 (IFNLR1), the "Cytokine signaling network" contained several important intracellular signaling components including those involved in regulating the inflammatory response such as Janus kinase 1 (JAK1) and GRB2-associated binder 1 (GAB1). Furthermore, this network contained several key negative regulators of inflammation such as Protein Inhibitor of Activated STAT3 (PIAS3), Suppressor of Cytokine Signaling 6 (SOCS6), and Atypical Chemokine Receptor 3 (ACKR3). The latter (ACKR3) has been shown to mediate chemokine sequestration, degradation, or transcytosis [59,60]. The "G protein - GPCR network", the "Chemotaxis network", and the "TLR2 response network" all contain key components that contribute to the recognition of microbe associated molecular patterns (MAMPs), chemotactic response of macrophages, and the regulation of the inflammatory response. Concordantly, functional enrichment analysis of the genes in these subnetworks revealed the top four enriched categories to be "GO Biological processes: Regulation of response to stimulus", "KEGG Pathway: JAK-STAT signaling pathway", GO Molecular Function: Signaling receptor activity", and "GO Biological Processes: G protein-coupled receptor signaling pathway" (Fig. 5C).

The Top 10 ORA Reactome Pathways significantly enriched in the downregulated DEGs, were all related to the cytokine and chemokine signaling response in the immune system (Fig. 5D). Consistently, STRING protein network analysis of the same genes, revealed the top four subnetworks (clusters 1–4) to comprise of inflammatory mediators known to be suppressed by glucocorticoids (Fig. 5E). The "Cytokine-chemokine network" comprised to a large extent of various macrophage-derived MAMP receptors (Toll-like receptors (TLR1, TLR4, TLR8)) and effector molecules. These effector molecules include interleukins (IL1A, IL1B, IL6, IL19, IL12B, IL16, IL18, IL33), cytokines (Chemokine (C-X-C motif) ligand 9 (CXCL9), CXCL10, CXCL11, Tumor necrosis factor (TNF) ligand superfamily member 10 (TNFSF10), Colony stimulating factor (CSF)), chemokines (Chemokine (C—C motif) ligand 1 (CCL1), CCL2, CCL5, CCL4L1, CCL19, CCL22), and their cognate receptors (IL36RN, CCR7, CX3CR2, CXCR5). It was additionally dominated by macrophage expressing co-stimulatory molecules that contribute to downstream macrophage-mediated effector T cell activation (Cluster of differentiation (CD)69, CD70, CD80, CD83, CD86, CD274, TNFRSF4, TNFRSF9) as well as molecules involved in lipid metabolism (prostaglandin synthesis) (FFAR2, PTGE2, PTGE4, PTGS2). The "IFN signaling network", the "Inflammation-modulatory network", and the "Signal transduction network" all contain key components that contribute to immune pathway signaling, downstream of the effector molecules and pattern recognition receptor (PRRs) in the "Cytokine-chemokine network". Key examples found in the "IFN signaling network" include the interferon (IFN) induced STAT1, STAT2, Guanylate Binding Protein 1–4 (GBP1, GBP2, GBP3, GBP4), IFNB1, IFN stimulated gene (ISG) 15, and 2'-5'-Oligoadenylate Synthase 1 (OAS1) that all contribute to the IFN signaling cascade. The main functional features of the proteins identified in the "Inflammation-modulatory network" are recognition of MAMPs and regulation of inflammation (Nucleotide Binding Oligomerization Domain Containing 2 (NOD2), TRAF3 interacting protein 3 (TRAF3IP3)), apoptosis (e.g., TNF Superfamily Member 15 (TNFSF15)), and macrophage bactericidal activity (Laccase Domain Containing 1 (LACC1). Finally, the "Signal transduction network" is characterized by proteins involved in maintenance of immune/inflammatory homeostasis. Notably, LYN (LYN Proto-Oncogene, Src Family Tyrosine Kinase), FYN (FYN Proto-Oncogene, Src Family Tyrosine Kinase) and SRC (SRC Proto-Oncogene, Src Family Tyrosine Kinase) have been shown to function as molecular switches that direct homeostasis and inflammation [61,62]. Consistent with these results, functional enrichment analysis of the genes in these subnetworks revealed the top three

Fig. 5. Genes classified as under intensified regulated expression are involved in the dexamethasone responsive immune regulation. (A) Enrichment analysis (Over-representation analysis, ORA) of Top 10 Reactome Pathways amongst the genes significantly upregulated by Dex (log2FC $\geq$ 0.58, p adj $\leq$ 0.05). The size of the dot represents the number of DEGs enriched in respective pathway in RNA-seq data. The enrichment ratio represents the number of enriched DEGs relative to the total number of genes in the respective pathway, and the color of the dot refers to the significance of enrichment (FDR). (B) STRING protein network analysis of significantly upregulated DEGs classified as intensified regulated, with the top four identified STRING subnetworks/clusters identified using Markov clustering (MCL). The surrounding donut color represents the enrichment categories plotted in (C). (C) The top four enriched categories (GO Biological Process, GO Molecular Function, and KEGG Pathway) in the subnetworks (B). *** FDR $\leq$ 0.001, was considered statistically significant. (D) Enrichment analysis (ORA) of Top 10 Reactome Pathways amongst genes significantly downregulated by dexamethasone (log2FC $\leq$ -0.58, p adj $\leq$ 0.05). The size of the dot represents the number of DEGs enriched in the respective pathway. The enrichment ratio represents the number of enriched DEGs relative to the total number of genes in the respective pathway, and the color of the dot refers to the significance of enrichment (FDR). (E) STRING protein network analysis of significantly downregulated DEGs classified as intensified regulated. Top four identified STRING subnetworks/clusters using Markov clustering (MCL). Surrounding donut colors represent the enrichment categories plotted in (F). (F) The top four enriched categories (GO Biological Process, KEGG Pathway, and Reactome Pathway) identified in the subnetworks (E). *** FDR $\leq$ 0.001 was considered statistically significant.

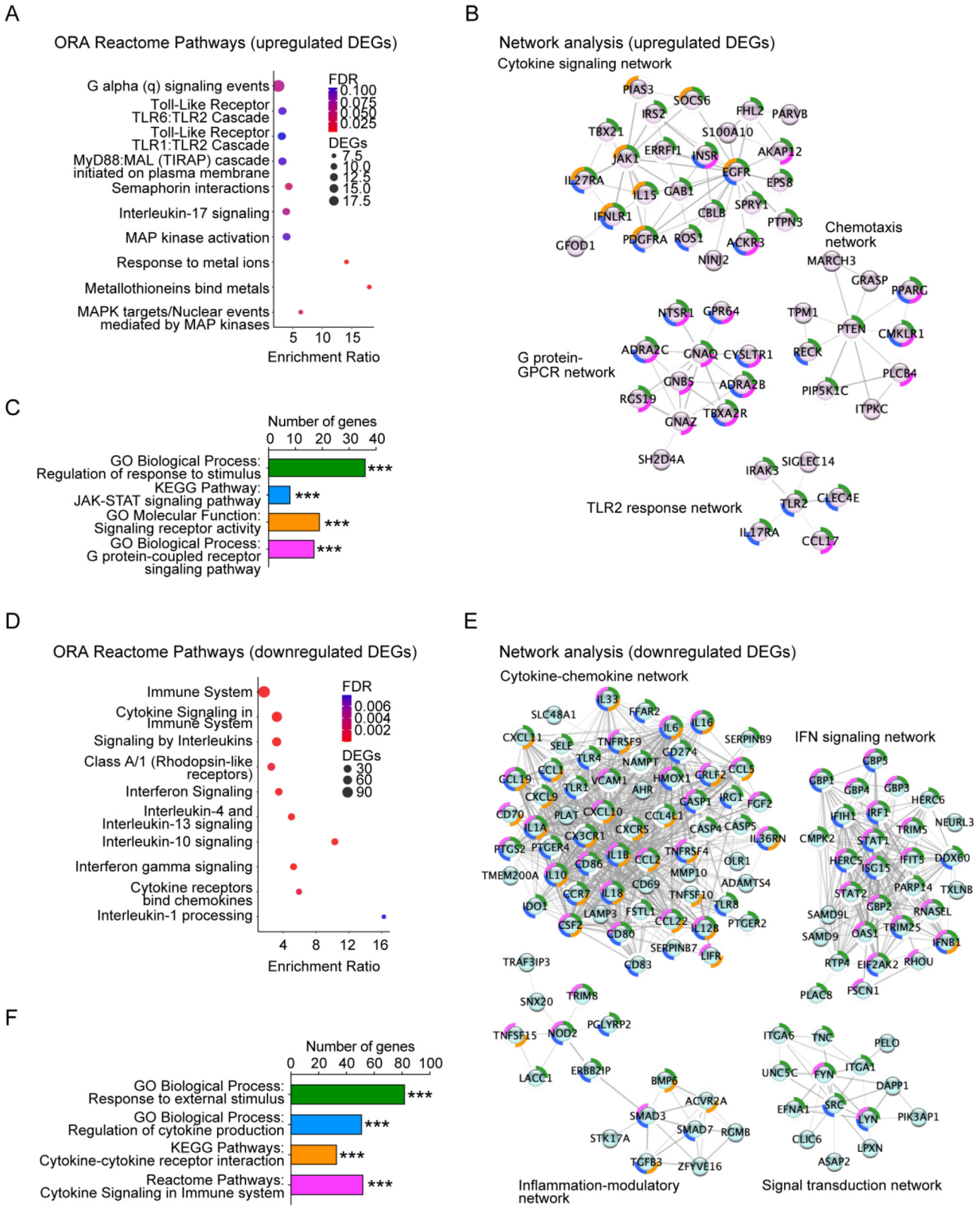
A
ORA Reactome Pathways (upregulated DEGs)
G alpha (q) signaling events
Toll-Like Receptor TLR6:TLR2 Cascade
Toll-Like Receptor TLR1:TLR2 Cascade
MyD88:MAL (TIRAP) cascade initiated on plasma membrane
Semaphorin interactions
Interleukin-17 signaling
MAP kinase activation
Response to metal ions
Metallothioneins bind metals
MAPK targets/Nuclear events mediated by MAP kinases
FDR
0.100
0.075
0.050
0.025
DEGs
7.5
10.0
12.5
15.0
17.5
5 10 15
Enrichment Ratio
B
Network analysis (upregulated DEGs)
Cytokine signaling network
PIAS3
SOCS6
IRS2
FHL2
PARVB
TBX21
S100A10
JAK1
ERRFI1
INSR
AKAP12
IL27RA
EGFR
EPS8
IL15
GAB1
SPRY1
IFNLR1
CBLB
PTPN3
GFOD1
PDGFRA
ROS1
ACKR3
NINJ2
Chemotaxis network
MARCH3
GRASP
PPARG
NTSR1
GPR64
TPM1
PTEN
CMKLR1
G protein-GPCR network
ADRA2C
GNAQ
CYSLTR1
RECK
GNB5
ADRA2B
PLCB4
RGS19
TBXA2R
PIP5K1C
GNAZ
ITPKC
SH2D4A
IRAK3
SIGLEC14
TLR2 response network
TLR2
CLEC4E
IL17RA
CCL17
C
Number of genes
0 10 20 30 40
GO Biological Process: Regulation of response to stimulus
KEGG Pathway: JAK-STAT signaling pathway
GO Molecular Function: Signaling receptor activity
GO Biological Process: G protein-coupled receptor singaling pathway
***
D
ORA Reactome Pathways (downregulated DEGs)
Immune System
Cytokine Signaling in Immune System
Signaling by Interleukins
Class A/1 (Rhodopsin-like receptors)
Interferon Signaling
Interleukin-4 and Interleukin-13 signaling
Interleukin-10 signaling
Interferon gamma signaling
Cytokine receptors bind chemokines
Interleukin-1 processing
FDR
0.006
0.004
0.002
DEGs
30
60
90
4 8 12 16
Enrichment Ratio
E
Network analysis (downregulated DEGs)
Cytokine-chemokine network
IL33
SLC48A1
FFAR2
IL6
IL16
CXCL11
SELE
TNFRSF9
SERPINB9
TLR4
CD274
NAMPT
CCL1
CCL5
CCL19
VCAM1
HMOX1
GRLF2
TLR1
AHR
CXCL9
CASP1
IRG1
FGF2
CD70
PLAT
CXCL10
CCL4L1
IL1A
CXCR5
CASP4
CASP5
IL36RN
CX3CR1
PTGS2
PTGER4
IL18
CCL2
TNFRSF4
CD86
OLR1
TMEM200A
IL10
MMP10
CD69
ADAMTS4
CCR7
IL18
TNFSF10
TLR8
IDO1
LAMP3
FSTL1
CCL22
PTGER2
CSF2
IL12B
CD80
SERPINB7
LIFR
CD83
TRAF3IP3
IFN signaling network
GBP5
GBP1
GBP4
GBP3
HERC6
IFIH1
IRF1
NEURL3
TRIM5
CMPK2
STAT1
HERC5
IFIT5
DDX60
ISG15
STAT2
PARP14
TXLNB
GBP2
SAMD9L
RNASEL
SAMD9
OAS1
TRIM25
IFNB1
RTP4
EIF2AK2
RHOU
PLAC8
FSCN1
SNX20
TRIM8
TNFSF15
NOD2
PGLYRP2
LACC1
ERBB2IP
BMP6
ACVR2A
SMAD3
SMAD7
RGMB
STK17A
TGFB3
ZFYVE16
Inflammation-modulatory network
ITGA6
TNC
PELO
UNC5C
FYN
ITGA1
DAPP1
EFNA1
SRC
LYN
PIK3AP1
CLIC6
LPXN
ASAP2
Signal transduction network
F
Number of genes
0 20 40 60 80 100
GO Biological Process: Response to external stimulus
GO Biological Process: Regulation of cytokine production
KEGG Pathways: Cytokine-cytokine receptor interaction
Reactome Pathways: Cytokine Signaling in Immune system
***

enriched categories to be "GO Biological Process: Response to external stimulus", "GO Biological Process: Regulation of cytokine production", and "KEGG Pathways: Cytokine-cytokine receptor interactions" (Fig. 5F). The top fourth enriched category found was "Reactome Pathways: Cytokine Signaling in Immune System", which had previously been identified as the most highly enriched Reactome Pathway (FDR < 2.220446e-16) in the full group of downregulated genes (Fig. 5A, F).

Moreover, having identified the "intensified" regulatory class as most prominent, we computationally identified the potential translational regulators that were enriched for a particular biological function. It is known that RBPs bind post-transcriptionally to target mRNAs and regulate their stability, distribution and translation into corresponding protein products [63,64]. We integrated expression data of "intensified" genes with RBP-RNA binding datasets based on eCLIP [65], iCLIP [66] and PAR-CLIP [67] experiments and provided by ENCODE [68] and POSTAR3 [42] web servers. We found 35 differentially expressed RBPs under the "intensified" category (Fig. S7A, Supplementary file 4). We also evaluated RBP - target regulatory relationships using a random forest based model (GENIE3) [43]. In this model, we identified ZFP36 and IGF2P2 as key potential translational regulators (RBPs) derived from a gene set involved in a biological process related to the regulation of cytokine production (Fig. S7B, Supplementary file 4). ZFP36 has been shown to act as a post-transcriptional anti-inflammatory modulator by suppressing the production of various pro-inflammatory cytokines, including TNF-alpha [69]. Recent studies have also revealed the posttranscriptional regulation of inflammatory processes by IGF2BP2 [70]. According to the change in translation efficiency pattern, targets for both RBPs include genes with increased or decreased translation efficiency (Fig. S7B). This suggests that ZFP36 and IGF2BP2 might act as either translational repressors or activators during the process of cytokine regulation by GCs.

Together, these results demonstrate that the dexamethasone-responsive genes that are categorized as "intensified" regulated, predominantly exhibit innate immune and immunomodulatory function that contribute to the macrophage response, as well as downstream macrophage-mediated activation of the adaptive response. Furthermore, data suggest that post-transcriptional mechanisms contribute to the expression of dexamethasone-responsive genes.

3.6. Pro-inflammatory leukotriene response and antigen presentation genes are buffered, while cell migration and apoptosis genes are under exclusively post-transcriptional regulation

Our differential expression analysis of the genes classified as "buffered" in the RNA-seq data identified 44 significantly upregulated DEGs and 92 downregulated DEGs (Fig. 4A). Gene-by-gene manual functional exploration of these genes identified six upregulated genes, and 26 downregulated genes, as exhibiting in immune or metabolic function (Fig. 6A). Microsomal Glutathione S-Transferase 2 (*MGST2*), which is involved in the production of pro-inflammatory leukotrienes (such as leukotriene C4, LTC4) and prostaglandin E, were found to activated by Dex [71,72]. Similarly, Signaling Receptor and Transporter of Retinol STRA6 (*STRA6*) and AKT Interacting Protein (*AKTIP*) were also activated. While *MGST2* contributes to inflammation, the retinal transporter *STRA6* contributes to the activation of Janus kinase 2 (JAK2) and its target STAT5, which ultimately increases the expression of the cytokine inhibitors *SOCS3* and *PPARG* [73,74]. Amongst the suppressed DEGs, key examples include *CD40*, *PARP9*, *ELOVL7*, *CXCL6*, *TLR6*, *PIKFYVE*, and *HLA-DQA1* that all contribute to immune-metabolic response, antigen presentation, or downstream B and T cells activation [75–79].

Subsequent STRING protein network analysis with Markov clustering (MCL) together with functional analysis identified two of the formed networks as comprising proteins involved in regulating antigen presentation ("Antigen presentation network") and interferon induction ("IFN induction regulatory network") (Fig. 6B). Enrichment analysis performed on the differentially expressed DEGs used for the networks consistently identified the top four enriched categories to be immune related: "GO Biological Process: Positive regulation of immune system process", "GO Biological Process: Immune response", "GO Biological Process: Response to molecule of bacterial origin", and "GO Biological Process: Regulation of defense response" (Fig. 6C). Together, this suggests that genes encoding proteins involved in antigen presentation and stimulation of T cell activation may be regulated on the transcriptional level and post-transcriptionally buffered, possibly as a safeguard mechanism against the rapid induction of aberrant downstream adaptive immune response activation.

Finally, differential expression analysis of the genes identified as exclusively translationally regulated ("exclusive") identified 103 DEGs as upregulated by Dex, and 58 as suppressed by Dex (Fig. 4B). These are genes whose expression is exclusively regulated in the translational level, exhibiting no significant changes on the transcriptional (mRNA) level nor a significant change in translational efficiency. Unlike our functional analysis of "intensified" and "buffered" genes, analysis of the exclusively translationally regulated genes only identified a handful of genes (*CCR2*, *IL24*, *CARD14*, *FABP3*, *SH3RF2*) associated with immunity (Fig. 6D, Supplementary file 3). Broadly, the exclusively translationally regulated genes were related to basic intracellular processes such as signaling and cytoskeletal changes (Fig. S8). Nevertheless, the immune related genes identified may be important. The CCR2 receptor mediates monocyte and macrophages chemotaxis, and cell movement toward sites of infection, through binding of CCL2 and CCL7 [80,81]. While Fatty acid binding protein 3 (FABP3) is involved in intracellular transport of long-chain fatty acids and their acyl-CoA esters; IL24, SH3 domain containing ring finger 2 (SH3RF2), and Caspase recruitment domain family member 14 (CARD14) have all been implicated in regulating cellular apoptosis [82–85]. Whereas *IL24* and *SH3RF2* that act as an inducer of apoptosis and as an anti-apoptotic regulator of the JNK pathway, respectively, were suppressed in response to Dex; *CARD14* expression was upregulated (Fig. 6D). CARD14, which not only protects cells against apoptosis, has also been shown to serve as a scaffolding protein that activates the inflammatory NF-κB and p38/JNK MAP kinase signaling pathways in a BCL10 and MALT1-dependent manner [84,86–88]. These observations are consistent with the shifts that stimulated monocytes undergo in the presence of external stimuli. While monocytes in general are relatively short lived and undergo spontaneous apoptosis in the absence of stimulation, pro-inflammatory stimulation (by e.g., LPS, IL-1β, and TNFα) results in inhibition of apoptosis [89].

Together, these results suggest that genes involved in processes governing cell movement and apoptosis in response to external stimuli are significantly regulated on the post-transcriptional level, possibly allowing for rapid changes prolonging cell viability and immune mobilization.

4. Discussion

In the context of host immunity, maintaining transcriptional and post-transcriptional gene regulation plays an essential role in the establishment and resolution of inflammation [90]. A dysregulated immune expression, stemming from aberrant upstream stream signaling or from alternations in the gene regulatory networks, can result in a disrupted immune homeostasis, excessive

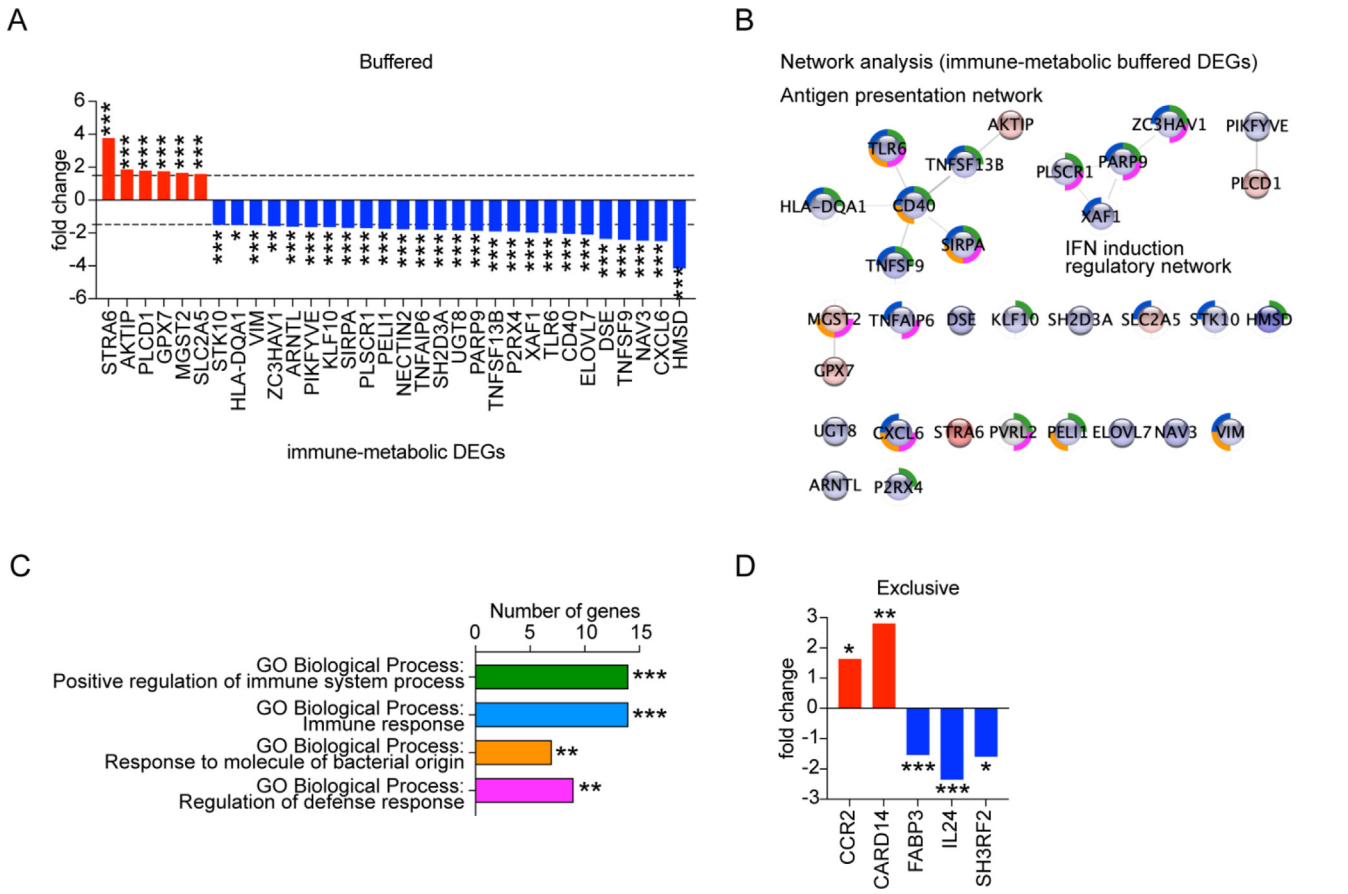

Fig. 6. Genes involved in the leukotriene response and antigen presentation are buffered, while genes regulating cell migration and apoptosis are exclusively post-transcriptionally regulated (A) Bar plot of Dex-responsive differentially expressed immune and metabolic genes (DEGs) under "buffered" expression regulation (RNA-seq). *** p adj ≤ 0.001, ** p adj ≤ 0.01, and * p adj ≤ 0.05 were considered statistically significant. (B) STRING protein network analysis of DEGs in (A) identified using Markov clustering (MCL). Fill color denote upregulated (red) or downregulated (blue) fold change expression. Surrounding donut color represent enrichment categories plotted in (C). (C) Top four enriched categories identified in the subnetworks (B). *** FDR ≤ 0.001, ** FDR ≤ 0.01 were considered statistically significant. (D) Bar plot of Dex-responsive differentially expressed immune genes (DEGs) under "exclusive" expression regulation (ribo-seq). *** p adj ≤ 0.001, ** p adj ≤ 0.01, and * p adj ≤ 0.05 were considered statistically significant. (For interpretation of the references to color in this figure legend, the reader is referred to the web version of this article.)

inflammation, reduced immune resolution, and associated altered phenotypes. In clinical contexts, GCs such as Dexamethasone, Prednisone or Cortisone are used to suppress excessive inflammation in a GR-dependent manner. Since GR is not merely an immune-specific transcriptional regulator, prolonged exposure of GCs does, however, come with a cost. Long-term use of GCs induces glucose intolerance and insulin resistance, adipocyte hypertrophy, osteoporosis, muscle and skin atrophy, glaucoma, impaired wound healing, steroid resistance, as well as various psychological side-effects including insomnia and depression [91–97]. Thus, novel insights into the gene regulatory networks that GR functions within, is key to more context-specific GC therapy. Generally, transcriptional changes coexist with mRNA export and stability regulation, translation efficiency, and protein stability, all of which influence the final protein output. In gene expression, translational control of specific mRNAs plays critical role, and numerous mechanisms have been identified to regulate translation [98]. For example, acute inflammatory responses may be suppressed by the rapid mRNA transcript degradation of cytokines, chemokines, enzymes, and other mediators [99]. Such post-transcriptional regulation is orchestrated by a diverse group of regulatory factors including RNA-binding proteins (RBP), microRNAs (miRNA) and other classes of small noncoding RNAs (sncRNA), which recognize and bind to sequences present in their target mRNAs [100–102]. Next generation sequencing methods such as RNA-seq, combined with ribo-seq, offers a quantitative approach to determine and understand the transcriptional and post-transcriptional gene regulation networks that GR acts within. When correlated with mRNA abundance, ribo-seq quantifies ribosome-protected fragments and allows the calculation of translation rates [103]. Here, we investigated the transcriptional and translational regulation by Dex-liganded GR, using a previously published computational method that integrates matched RNA-seq and ribo-seq data to subcategorize genes as forwarded, intensified, buffered, or exclusively (exclusive) translationally regulated [24]. Dex treatment of LPS-stimulated macrophages displayed genome-wide translated ORFs with ribosome profiling when combined with quantitative mRNA sequencing. Our list includes >90 % protein coding ORFs that comprise CDS (14,266 genes), uORF (416 genes), intORF (10 genes) and dORF (20genes) (Fig. 2G). As reported by recent studies, both uORF and dORF are essential in modulating the translation of CDS [104–107]. The small noncoding translated ORFs identified in our study may represent a significant source of peptides, which warrants additional investigation. Several recent studies highlighted the importance of these un-annotated ORFs which might encode micro-proteins with essential regulatory functions [108–111]. Importantly, 490 non-canonical ORFs were already annotated in a recent standardized ribo-seq ORF catalog [112]. The greatest interest in our study is determining the regulatory class of protein coding genes (CDS) using the deltaTE approach (Fig. 3D-G). Here

we found that in Dex treated LPS-stimulated macrophages, the majority of the significantly differentially expressed genes were regulated on both the transcriptional and translational levels (intensified). Consistent with the immune suppressive function of the GC-GR axis, network and enrichment analyses identify these as pro-inflammatory immune effector and immunomodulatory molecules. While Dex treatment resulted in suppression of immune effectors such as cytokines (interferons and interleukins), chemokines, TLRs, co-stimulatory markers, and intracellular pathway components; several key negative regulators of inflammation (*PIAS3*, *SOCS6*, and *ACKR3*) were conversely upregulated by Dex. Notably, in airway epithelial cells, pro-inflammatory genes such as Tumor necrosis factor alpha (*TNFα*), *IL6*, *IL4Rα*, inducible nitric oxide synthase (*iNOS*), and *CCL2*, *CCL7*, *CCL11* have all been observed to be post-transcriptionally regulated in a GC-dependent manner [15–18,113,114]. In the case of the chemotactic *CCL2*, GR has been shown to interact with Proline-rich nuclear receptor coregulator protein 2 (PNRC2) in a ligand-dependent manner, recruiting Upstream frame-shift 2 (UFP2), triggering a rapid *CCL2* mRNA degradation and reducing chemotaxis ('GR-mediated mRNA decay') in THP-1 cells [115]. While these select examples suggest a role for GC/GR-dependent post-transcriptional regulation, our study now sheds light on the impact of global post-transcriptional regulation by GCs in macrophage inflammatory settings. Predicting a post-transcriptional regulatory network model, we infer a potential role of ribosome binding proteins (RBPs) in translation control of GR target mRNAs during the regulation of inflammatory cytokine production (Fig. S7).

Amongst the upregulated intensified genes, *TLR2* was found to form an antimicrobial response protein network with *IRAK3*, *SIGLEC14*, *CLECL4E*, *IL17RA*, and the antimicrobial *CCL17* ("TLR2 response network"). Like TLR2, CLEC4E functions as a PRR for bacterial and fungal MAMPs as well as damage-associate molecular patterns (DAMPs) [115,116]. Notably, in macrophages, *Listeria monocytogenes* activates CLEC5A and TLR2 simultaneously to activate both the MyD88-p38 and Syk-AKT signaling pathways, which induces inflammasome activation and production of IL-1β and IL17A resulting in production of T cell receptor (TCR) γβ T cells, vital to the initial inflammatory and immune response [117].

In the presence of an infection, innate immune effector responses must be rapid and potent to counteract the developing infection. Our observations that pro-inflammatory effector molecules and molecules regulating or contributing to these responses are under intensified regulation are consistent with their function as antimicrobial agents and promoters of chemotaxis of other immune cells. Likewise, we find that genes involved in cytoskeletal rearrangement and apoptosis are exclusively regulated on the translational level, allowing for rapid changes in protein abundance to maintain these functions. Although the initial pro-inflammatory response requires a potent induction, downstream responses governing the activation and regulation of the adaptive B and T cell response, require a multi-layer regulation. In line with this notion, our data suggests that the downregulated *CD40*, *PARP9*, *CXCL6*, *TLR6*, *PIKFYVE*, and *HLA-DQA1* belong to the category of "buffered" genes that exhibit a significant change on the transcriptional level and a counteracting significant translational efficiency and are therefore regulated on both the transcriptional and translational levels. For instance, expression of CD40 on macrophages allows for interaction with CD40 ligand (CD40LG) on B and T cells, which induces memory B cell development as well as T cell-dependent Ig class switching [75,76]. Our observations that suppression of Toll-like receptor 6 (*TLR6*), Major Histocompatibility Complex (MHC), Class II, DQ Alpha 1 (*HLA-DQA1*), and Phosphatinositide kinase, FYVE-type zinc finger containing (*PIKFYVE*) which plays a key role in MHC class II antigen presentation (to T cells), all suggest that Dex reduces macrophage antigen presentation and subsequent T cell response [77]. Further, reduction of Poly (ADP-Ribose) Polymerase Family Member 9 (*PARP9*) and *CXCL6* suggests a reduction of pro-inflammatory cytokine and chemokine production [78,79]. Taken together, we define a global transcriptional and translational regulatory profile for GR-target genes in human macrophages. In particular, the translational control may play a pertinent role in inflammatory genes suppression by GR.

5. Conclusion

In this study, a ribosome profiling approach combined with mRNA sequencing was used to classify Dex responsive LPS-stimulated genes into various translational regulatory classes based on fold changes in mRNA, ribosome-protected RNA fragments, and translation efficiency. In this line, the THP-1 derived macrophages serve as a reproducible model system for gaining new mechanistic insight into the function of the GC-GR axis in immune regulation. The translation efficiency was calculated by normalizing an average of ribosome footprint density by the abundance of the gene's mRNA. The relative direction of change in mRNA abundance and translation efficiency was used to classify genes. Our analysis in Dex and LPS stimulated macrophages resulted in categorization of Dex responsive genes mainly into four distinct regulatory classes: forwarded, exclusive, intensified, and buffered. Transcriptional regulation drives translationally "forwarded" genes, whereas "exclusive" genes are governed by translational control. Genes belonging to "intensified" class make up the majority of differentially expressed genes, and these genes are both regulated by transcription and translation. Importantly, gene enrichment and STRING protein network analysis revealed a vast array of Dex-GR target genes in the intensified regulatory class that are involved in macrophage inflammation modulation. In this regard, however, much remains to be learned about mechanisms of translational control [10,118–123]. Nevertheless, an important step toward this goal is to characterize the post-transcriptional regulation of early GR responsive genes (e.g. RBPs) in primary murine and human macrophages, which is linked to protein synthesis inhibition in response to Dex stimulation. Importantly, our ribosome profiling in macrophages has revealed that a large number of non-canonical ORFs are translated outside of the annotated coding sequences. Further characterization of these small ORFs may alter our understanding of translational regulatory mechanisms in several biological processes of medical relevance. Thus, further research into the global translational regulatory mechanisms that underpins the GR anti-inflammatory response could pave the way for the development of improved and safer immunomodulatory therapeutic regimens.

Data availability

All NGS datasets generated for this study are accessible though GEO under accession number GSE208041.

Declaration of Competing Interest

The authors declare that they have no known competing financial interests or personal relationships that could have appeared to influence the work reported in this paper.

Acknowledgements

We sincerely thank S. Regn, I. Guderian, T. Horn, B. Haderlein and Claudia Langnick (MDC) for assistance. This work has been supported by funding from the ERC (ERC StG 2014 SILENCE), the Else Kroener Fresenius Foundation (EKFS) and the German Research

Foundation DFG (CRC1064 Chromatin Dynamics) to NHU. NH is recipient of an ERC advanced grant under the European Union's Horizon 2020 research and innovation programme (grant agreement n° AdG788970), and a grant from the Leducq Foundation (16CVD03). We apologize to all authors whose work could not be cited due to space constraints.

Author contributions

SAA performed the data processing, QC analysis for Ribo-seq data and deltaTE analysis for gene regulatory classification. WD performed enrichment analysis, STRING network analysis, and performed downstream biological interpretation. APS performed the cell culture experiments. SB prepared the sequencing libraries for Ribo-seq and RNA-seq. JRO performed the data processing and analysis to predict the translated open reading frames. JRO, SvH, and NH provided relevant advice and technical details. SAA, WD, and NHU wrote the manuscript.

Appendix A. Supplementary data

Supplementary data to this article can be found online at https://doi.org/10.1016/j.csbj.2022.09.042.

References

[1] Adeli K. Translational control mechanisms in metabolic regulation: critical role of RNA binding proteins, microRNAs, and cytoplasmic RNA granules. Am J Physiol Endocrinol Metab 2011;301(6):E1051–64. https://doi.org/10.1152/ajpendo.00399.2011.
[2] Ingolia NT, Ghaemmaghami S, Newman JR, Weissman JS. Genome-wide analysis in vivo of translation with nucleotide resolution using ribosome profiling. Science 2009;324(5924):218–23. https://doi.org/10.1126/science.1168978.
[3] Besedovsky HO, del Rey A. Regulating inflammation by glucocorticoids. Nat Immunol 2006;7(6):537. https://doi.org/10.1038/ni0606-537.
[4] Flammer JR et al. The type I interferon signaling pathway is a target for glucocorticoid inhibition. Mol Cell Biol 2010;30(19):4564–74. https://doi.org/10.1128/MCB.00146-10.
[5] Frieri M. Corticosteroid effects on cytokines and chemokines. Allergy Asthma Proc 1999;20(3):147–59. https://doi.org/10.2500/108854199778553082.
[6] Cruz-Topete D, Cidlowski JA. One hormone, two actions: anti- and pro-inflammatory effects of glucocorticoids. NeuroImmunoModulation 2015;22(1–2):20–32. https://doi.org/10.1159/000362724.
[7] Muzikar KA, Nickols NG, Dervan PB. Repression of DNA-binding dependent glucocorticoid receptor-mediated gene expression. Proc Natl Acad Sci U S A 2009;106(39):16598–603. https://doi.org/10.1073/pnas.0909192106.
[8] Presman DM, Ganguly S, Schiltz RL, Johnson TA, Karpova TS, Hager GL. DNA binding triggers tetramerization of the glucocorticoid receptor in live cells,. Proc Natl Acad Sci U S A 2016;113(29):8236–41. https://doi.org/10.1073/pnas.1606774113.
[9] Jubb AW, Boyle S, Hume DA, Bickmore WA. Glucocorticoid receptor binding induces rapid and prolonged large-scale chromatin decompaction at multiple target loci. Cell Rep 2017;21(11):3022–31. https://doi.org/10.1016/j.celrep.2017.11.053.
[10] Strickland BA, Ansari SA, Dantoft W, Uhlenhaut NH. How to tame your genes: mechanisms of inflammatory gene repression by glucocorticoids. FEBS Lett 2022. https://doi.org/10.1002/1873-3468.14409.
[11] Reily MM, Pantoja C, Hu X, Chinenov Y, Rogatsky I. The GRIP1:IRF3 interaction as a target for glucocorticoid receptor-mediated immunosuppression. EMBO J 2006;25(1):108–17. https://doi.org/10.1038/sj.emboj.7600919.
[12] Rollins DA et al. Glucocorticoid-induced phosphorylation by CDK9 modulates the coactivator functions of transcriptional cofactor GRIP1 in macrophages. Nat Commun 2017;8(1):1739. https://doi.org/10.1038/s41467-017-01569-2.
[13] Dobrovolna J, Chinenov Y, Kennedy MA, Liu B, Rogatsky I. Glucocorticoid-dependent phosphorylation of the transcriptional coregulator GRIP1. Mol Cell Biol 2012;32(4):730–9. https://doi.org/10.1128/MCB.06473-11.
[14] Chinenov Y et al. Role of transcriptional coregulator GRIP1 in the anti-inflammatory actions of glucocorticoids. Proc Natl Acad Sci U S A 2012;109(29):11776–81. https://doi.org/10.1073/pnas.1206059109.
[15] Stellato C. Glucocorticoid actions on airway epithelial responses in immunity: functional outcomes and molecular targets quiz 1264-5. J Allergy Clin Immunol 2007;120(6):1247–63. https://doi.org/10.1016/j.jaci.2007.10.041.
[16] Tobler A, Meier R, Seitz M, Dewald B, Baggiolini M, Fey MF. Glucocorticoids downregulate gene expression of GM-CSF, NAP-1/IL-8, and IL-6, but not of M-CSF in human fibroblasts. Blood 1992;79(1):45–51.
[17] Smoak K, Cidlowski JA. Glucocorticoids regulate tristetraprolin synthesis and posttranscriptionally regulate tumor necrosis factor alpha inflammatory signaling. Mol Cell Biol 2006;26(23):9126–35. https://doi.org/10.1128/MCB.00679-06.
[18] Stellato C et al. Differential regulation of epithelial-derived C-C chemokine expression by IL-4 and the glucocorticoid budesonide. J Immunol 1999;163(10):5624–32.
[19] Lund ME, To J, O'Brien BA, Donnelly S. The choice of phorbol 12-myristate 13-acetate differentiation protocol influences the response of THP-1 macrophages to a pro-inflammatory stimulus. J Immunol Methods 2016;430:64–70. https://doi.org/10.1016/j.jim.2016.01.012.
[20] Chanput W, Mes JJ, Wichers HJ. THP-1 cell line: an in vitro cell model for immune modulation approach. Int Immunopharmacol 2014;23(1):37–45. https://doi.org/10.1016/j.intimp.2014.08.002.
[21] Alvi A et al. Concurrent proinflammatory and apoptotic activity of a Helicobacter pylori protein (HP986) points to its role in chronic persistence. PLoS ONE 2011;6(7):e22530.
[22] Yang L et al. Oleoylethanolamide exerts anti-inflammatory effects on LPS-induced THP-1 cells by enhancing PPARα signaling and inhibiting the NF-κB and ERK1/2/AP-1/STAT3 pathways. Sci Rep 2016;6:34611. https://doi.org/10.1038/srep34611.
[23] Genin M, Clement F, Fattaccioli A, Raes M, Michiels C. M1 and M2 macrophages derived from THP-1 cells differentially modulate the response of cancer cells to etoposide. BMC Cancer 2015;15:577. https://doi.org/10.1186/s12885-015-1546-9.
[24] Chothani S et al. deltaTE: detection of translationally regulated genes by integrative analysis of Ribo-seq and RNA-seq data. Curr Protoc Mol Biol 2019;129(1). https://doi.org/10.1002/cpmb.108.
[25] McGlincy NJ, Ingolia NT. Transcriptome-wide measurement of translation by ribosome profiling. Methods 2017;126:112–29. https://doi.org/10.1016/j.ymeth.2017.05.028.
[26] van Heesch S et al. The translational landscape of the human heart. Cell 2019;178(1):242–260.e29. https://doi.org/10.1016/j.cell.2019.05.010.
[27] Gaertner B et al. "A human ESC-based screen identifies a role for the translated lncRNA. Elife 2020;9(08):03. https://doi.org/10.7554/eLife.58659.
[28] Schneider-Lunitz V, Ruiz-Orera J, Hubner N, van Heesch S. Multifunctional RNA-binding proteins influence mRNA abundance and translational efficiency of distinct sets of target genes. PLoS Comput Biol 2021;17(12). https://doi.org/10.1371/journal.pcbi.1009658.
[29] Langmead B, Salzberg SL. "Fast gapped-read alignment with Bowtie 2. Nat Methods 2012;9(4):357–9. https://doi.org/10.1038/nmeth.1923.
[30] Dobin A et al. "STAR: ultrafast universal RNA-seq aligner. Bioinformatics 2013;29(1):15–21. https://doi.org/10.1093/bioinformatics/bts635.
[31] Calviello L, Hirsekorn A, Ohler U. Quantification of translation uncovers the functions of the alternative transcriptome. Nat Struct Mol Biol 2020;27(8):717–25. https://doi.org/10.1038/s41594-020-0450-4.
[32] Love MI, Huber W, Anders S. "Moderated estimation of fold change and dispersion for RNA-seq data with DESeq2. Genome Biol 2014;15(12):550. https://doi.org/10.1186/s13059-014-0550-8.
[33] Zhang P et al. "Genome-wide identification and differential analysis of translational initiation. Nat Commun 2017;8(1):1749. https://doi.org/10.1038/s41467-017-01981-8.
[34] Lauria F, Tebaldi T, Bernabò P, Groen EJN, Gillingwater TH, Viero G. riboWaltz: Optimization of ribosome P-site positioning in ribosome profiling data. PLoS Comput Biol 2018;14(8). https://doi.org/10.1371/journal.pcbi.1006169.
[35] Liao Y, Smyth GK, Shi W. featureCounts: an efficient general purpose program for assigning sequence reads to genomic features. Bioinformatics 2014;30(7):923–30. https://doi.org/10.1093/bioinformatics/btt656.
[36] Kuleshov MV et al. Enrichr: a comprehensive gene set enrichment analysis web server 2016 update. Nucleic Acids Res 2016;44(W1):W90–7. https://doi.org/10.1093/nar/gkw377.
[37] Paczkowska M et al. Integrative pathway enrichment analysis of multivariate omics data. Nat Commun 2020;11(1):735. https://doi.org/10.1038/s41467-019-13983-9.
[38] Fabregat A et al. The Reactome pathway Knowledgebase. Nucleic Acids Res Jan 2016;44(D1):D481–7. https://doi.org/10.1093/nar/gkv1351.
[39] Ashburner M et al. Gene ontology: tool for the unification of biology. The Gene Ontology Consortium. Nat Genet 2000;25(1):25–9. https://doi.org/10.1038/75556.
[40] Reimand J, Kull M, Peterson H, Hansen J, Vilo J, g:Profiler–a web-based toolset for functional profiling of gene lists from large-scale experiments, Nucleic Acids Res, 35(Web Server issue), pp. W193-200, 2007, doi: 10.1093/nar/gkm226.
[41] Won S, Morris N, Lu Q, Elston RC. "Choosing an optimal method to combine P-values. Stat Med 2009;28(11):1537–53. https://doi.org/10.1002/sim.3569.
[42] Zhao W et al. POSTAR3: an updated platform for exploring post-transcriptional regulation coordinated by RNA-binding proteins. Nucleic Acids Res 2022;50(D1):D287–94. https://doi.org/10.1093/nar/gkab702.
[43] Huynh-Thu VA, Irrthum A, Wehenkel L, Geurts P. Inferring regulatory networks from expression data using tree-based methods. PLoS One 2010;5(9). https://doi.org/10.1371/journal.pone.0012776.
[44] Csardi G, Nepusz T, "The igraph software package for complex network research. ed. InterJournal: Vol. Complex Systems, 2006, p. 1695.

[45] Gustavsen JA, Pai S, Isserlin R, Demchak B, Pico AR. RCy3: Network biology using Cytoscape from within R. F1000Res 2019;8:1774. https://doi.org/10.12688/f1000research.20887.3.
[46] Liao Y, Wang J, Jaehnig EJ, Shi Z, Zhang B. WebGestalt 2019: gene set analysis toolkit with revamped UIs and APIs. Nucl Acids Res 2019;47(W1):W199–205. https://doi.org/10.1093/nar/gkz401.
[47] Shannon P et al. "Cytoscape: a software environment for integrated models of biomolecular interaction networks. Genome Res Nov 2003;13(11):2498–504. https://doi.org/10.1101/gr.1239303.
[48] Doncheva NT, Morris JH, Gorodkin J, Jensen LJ. Cytoscape StringApp: network analysis and visualization of proteomics data. J Proteome Res 2019;18 (2):623–32. https://doi.org/10.1021/acs.jproteome.8b00702.
[49] Morris JH et al. clusterMaker: a multi-algorithm clustering plugin for Cytoscape. BMC Bioinformatics 2011;12:436. https://doi.org/10.1186/1471-2105-12-436.
[50] Enright AJ, Van Dongen S, Ouzounis CA. An efficient algorithm for large-scale detection of protein families. Nucleic Acids Res 2002;30(7):1575–84. https://doi.org/10.1093/nar/30.7.1575.
[51] Shepherd JC. Method to determine the reading frame of a protein from the purine/pyrimidine genome sequence and its possible evolutionary justification. Proc Natl Acad Sci U S A 1981;78(3):1596–600. https://doi.org/10.1073/pnas.78.3.1596.
[52] Yin C, Yau SS. "Prediction of protein coding regions by the 3-base periodicity analysis of a DNA sequence. J Theor Biol 2007;247(4):687–94. https://doi.org/10.1016/j.jtbi.2007.03.038.
[53] Zhou J, Lancaster L, Donohue JP, Noller HF. "How the ribosome hands the A-site tRNA to the P site during EF-G-catalyzed translocation. Science 2014;345 (6201):1188–91. https://doi.org/10.1126/science.1255030.
[54] Ahmed N, Sormanni P, Ciryam P, Vendruscolo M, Dobson CM, O'Brien EP. Identifying A- and P-site locations on ribosome-protected mRNA fragments using Integer Programming. Sci Rep 2019;9(1):6256. https://doi.org/10.1038/s41598-019-42348-x.
[55] Jansen M, de Moor CH, Sussenbach JS, van den Brande JL. "Translational control of gene expression. Pediatr Res Jun 1995;37(6):681–6. https://doi.org/10.1203/00006450-199506000-00001.
[56] Sohn EJ, Moon HJ, Lim JK, Kim DS, Kim JH. Regulation of the protein stability and transcriptional activity of OCT4 in stem cells. Adv Biol Regul 2021;79. https://doi.org/10.1016/j.jbior.2020.100777.
[57] McShane E, Selbach M. Gene expression: degrade to derepress. EMBO J 2014;33(5):407–8. https://doi.org/10.1002/embj.201387752.
[58] Wu Q et al. Translation affects mRNA stability in a codon-dependent manner in human cells. Elife 2019;8(04):23. https://doi.org/10.7554/eLife.45396.
[59] Locati M et al. Silent chemoattractant receptors: D6 as a decoy and scavenger receptor for inflammatory CC chemokines. Cytokine Growth Factor Rev 2005;16(6):679–86. https://doi.org/10.1016/j.cytogfr.2005.05.003.
[60] Bachelerie F et al. New nomenclature for atypical chemokine receptors. Nat Immunol 2014;15(3):207–8. https://doi.org/10.1038/ni.2812.
[61] Hu X, Wang H, Han C, Cao X. Src promotes anti-inflammatory (M2) macrophage generation via the IL-4/STAT6 pathway. Cytokine 2018;111:209–15. https://doi.org/10.1016/j.cyto.2018.08.030.
[62] Mkaddem SB et al. Lyn and Fyn function as molecular switches that control immunoreceptors to direct homeostasis or inflammation. Nat Commun 2017;8(1):246. https://doi.org/10.1038/s41467-017-00294-0.
[63] Matoulkova E, Michalova E, Vojtesek B, Hrstka R. "The role of the 3' untranslated region in post-transcriptional regulation of protein expression in mammalian cells. RNA Biol 2012;9(5):563–76. https://doi.org/10.4161/rna.20231.
[64] Sonenberg N, Hinnebusch AG. Regulation of translation initiation in eukaryotes: mechanisms and biological targets. Cell 2009;136(4):731–45. https://doi.org/10.1016/j.cell.2009.01.042.
[65] Van Nostrand EL et al. Robust transcriptome-wide discovery of RNA-binding protein binding sites with enhanced CLIP (eCLIP). Nat Methods 2016;13 (6):508–14. https://doi.org/10.1038/nmeth.3810.
[66] Huppertz I et al. "iCLIP: protein-RNA interactions at nucleotide resolution. Methods 2014;65(3):274–87. https://doi.org/10.1016/j.ymeth.2013.10.011.
[67] Danan C, Manickavel S, Hafner M. "PAR-CLIP: a method for transcriptome-wide identification of RNA binding protein interaction sites. Methods Mol Biol 2016;1358:153–73. https://doi.org/10.1007/978-1-4939-3067-8_10.
[68] Luo Y et al. New developments on the Encyclopedia of DNA Elements (ENCODE) data portal. Nucl Acids Res 2020;48(D1):D882–9. https://doi.org/10.1093/nar/gkz1062.
[69] Makita S, Takatori H, Nakajima H. Post-transcriptional regulation of immune responses and inflammatory diseases by RNA-binding ZFP36 family proteins. Front Immunol 2021;12:. https://doi.org/10.3389/fimmu.2021.711633711633.
[70] Schymik HS, Dahlem C, Barghash A, Kiemer AK. Comment on: The m6A Reader IGF2BP2 Regulates Macrophage Phenotypic Activation and Inflammatory Diseases by Stabilizing TSC1 and PPARγ. Adv Sci (Weinh) 2022;9(8). https://doi.org/10.1002/advs.202104372.
[71] Ahmad S, Niegowski D, Wetterholm A, Haeggström JZ, Morgenstern R, Rinaldo-Matthis A. "Catalytic characterization of human microsomal glutathione S-transferase 2: identification of rate-limiting steps. Biochemistry 2013;52(10):1755–64. https://doi.org/10.1021/bi3014104.
[72] Dvash E, Har-Tal M, Barak S, Meir O, Rubinstein M. Leukotriene C4 is the major trigger of stress-induced oxidative DNA damage. Nat Commun 2015;6:10112. https://doi.org/10.1038/ncomms10112.
[73] Berry DC, O'Byrne SM, Vreeland AC, Blaner WS, Noy N. Cross talk between signaling and vitamin A transport by the retinol-binding protein receptor STRA6. Mol Cell Biol 2012;32(15):3164–75. https://doi.org/10.1128/MCB.00505-12.
[74] Berry DC, Jin H, Majumdar A, Noy N. "Signaling by vitamin A and retinol-binding protein regulates gene expression to inhibit insulin responses. Proc Natl Acad Sci U S A 2011;108(11):4340–5. https://doi.org/10.1073/pnas.1011115108.
[75] Takada YK, Yu J, Shimoda M, Takada Y. Integrin Binding to the Trimeric Interface of CD40L Plays a Critical Role in CD40/CD40L Signaling. J Immunol 2019;203(5):1383–91. https://doi.org/10.4049/jimmunol.1801630.
[76] Jabara HH, Weng Y, Sannikova T, Geha RS. TRAF2 and TRAF3 independently mediate Ig class switching driven by CD40. Int Immunol 2009;21(4):477–88. https://doi.org/10.1093/intimm/dxp013.
[77] Baranov MV et al. The Phosphoinositide Kinase PIKfyve Promotes Cathepsin-S-Mediated Major Histocompatibility Complex Class II Antigen Presentation. iScience 2019;11:160–77. https://doi.org/10.1016/j.isci.2018.12.015.
[78] Linge HM, Collin M, Nordenfelt P, Mörgelin M, Malmsten M, Egesten A. The human CXC chemokine granulocyte chemotactic protein 2 (GCP-2)/CXCL6 possesses membrane-disrupting properties and is antibacterial. Antimicrob Agents Chemother Jul 2008;52(7):2599–607. https://doi.org/10.1128/AAC.00028-08.
[79] Iwata H et al. PARP9 and PARP14 cross-regulate macrophage activation via STAT1 ADP-ribosylation. Nat Commun 2016;7:12849. https://doi.org/10.1038/ncomms12849.
[80] Wang JM, Hishinuma A, Oppenheim JJ, Matsushima K. Studies of binding and internalization of human recombinant monocyte chemotactic and activating factor (MCAF) by monocytic cells. Cytokine 1993;5(3):264–75. https://doi.org/10.1016/1043-4666(93)90014-v.
[81] Franci C, Wong LM, Van Damme J, Proost P, Charo IF. Monocyte chemoattractant protein-3, but not monocyte chemoattractant protein-2, is a functional ligand of the human monocyte chemoattractant protein-1 receptor. J Immunol 1995;154(12):6511–7.
[82] Islam A et al. Fatty Acid Binding Protein 3 Is Involved in n-3 and n-6 PUFA transport in mouse trophoblasts. J Nutr 2014;144(10):1509–16. https://doi.org/10.3945/jn.114.197202.
[83] Wilhelm M et al. Sh3rf2/POSHER protein promotes cell survival by ring-mediated proteasomal degradation of the c-Jun N-terminal kinase scaffold POSH (Plenty of SH3s) protein. J Biol Chem 2012;287(3):2247–56. https://doi.org/10.1074/jbc.M111.269431.
[84] Bertin J et al. "CARD11 and CARD14 are novel caspase recruitment domain (CARD)/membrane-associated guanylate kinase (MAGUK) family members that interact with BCL10 and activate NF-kappa B. J Biol Chem 2001;276 (15):11877–82. https://doi.org/10.1074/jbc.M010512200.
[85] Persaud L, et al., IL-24 Promotes Apoptosis through cAMP-Dependent PKA Pathways in Human Breast Cancer Cells, Int J Mol Sci, vol. 19, no. 11, 2018, doi: 10.3390/ijms19113561.
[86] Scudiero I, Zotti T, Ferravante A, Vessichelli M, Vito P, Stilo R. Alternative splicing of CARMA2/CARD14 transcripts generates protein variants with differential effect on NF-κB activation and endoplasmic reticulum stress-induced cell death. J Cell Physiol 2011;226(12):3121–31. https://doi.org/10.1002/jcp.22667.
[87] Afonina IS et al. The paracaspase MALT1 mediates CARD14-induced signaling in keratinocytes. EMBO Rep 2016;17(6):914–27. https://doi.org/10.15252/embr.201642109.
[88] Howes A et al. Psoriasis mutations disrupt CARD14 autoinhibition promoting BCL10-MALT1-dependent NF-κB activation. Biochem J 2016;473 (12):1759–68. https://doi.org/10.1042/BCJ20160270.
[89] Zhao C et al. The CD14(+/low)CD16(+) monocyte subset is more susceptible to spontaneous and oxidant-induced apoptosis than the CD14(+)CD16(-) subset. Cell Death Dis 2010;1. https://doi.org/10.1038/cddis.2010.69.
[90] Anderson P. "Post-transcriptional regulons coordinate the initiation and resolution of inflammation. Nat Rev Immunol 2010;10(1):24–35. https://doi.org/10.1038/nri2685.
[91] Kadmiel M, Cidlowski JA. "Glucocorticoid receptor signaling in health and disease. Trends Pharmacol Sci 2013;34(9):518–30. https://doi.org/10.1016/j.tips.2013.07.003.
[92] Hartmann K et al. Molecular actions of glucocorticoids in cartilage and bone during health, disease, and steroid therapy. Physiol Rev 2016;96(2):409–47. https://doi.org/10.1152/physrev.00011.2015.
[93] Brown ES, Chandler PA. Mood and cognitive changes during systemic corticosteroid therapy. Prim Care Companion J Clin Psychiatry 2001;3 (1):17–21. https://doi.org/10.4088/pcc.v03n0104.
[94] Rice JB, White AG, Scarpati LM, Wan G, Nelson WW. Long-term systemic corticosteroid exposure: a systematic literature review. Clin Ther 2017;39 (11):2216–29. https://doi.org/10.1016/j.clinthera.2017.09.011.
[95] van Staa TP, Leufkens HG, Abenhaim L, Zhang B, Cooper C. Oral corticosteroids and fracture risk: relationship to daily and cumulative doses. Rheumatology (Oxford) 2000;39(12):1383–9. https://doi.org/10.1093/rheumatology/39.12.1383.
[96] Silverman MN, Sternberg EM. Glucocorticoid regulation of inflammation and its functional correlates: from HPA axis to glucocorticoid receptor dysfunction. Ann N Y Acad Sci 2012;1261:55–63. https://doi.org/10.1111/j.1749-6632.2012.06633.x.
[97] Dawson C, Dhanda A, Conway-Campbell B, Dimambro A, Lightman S, Dayan C. NFκB and glucocorticoid receptor activity in steroid resistance. J Recept

Signal Transduct Res 2012;32(1):29–35. https://doi.org/10.3109/10799893.2011.641977.
[98] Harvey RF et al. Trans-acting translational regulatory RNA binding proteins. Wiley Interdiscip Rev RNA 2018;9(3). https://doi.org/10.1002/wrna.1465.
[99] Uchida Y, Chiba T, Kurimoto R, Asahara H. Post-transcriptional regulation of inflammation by RNA-binding proteins via cis-elements of mRNAs. J Biochem 2019;166(5):375–82. https://doi.org/10.1093/jb/mvz067.
[100] Balasubramanian D, Vanderpool CK. New developments in post-transcriptional regulation of operons by small RNAs. RNA Biol 2013;10 (3):337–41. https://doi.org/10.4161/rna.23696.
[101] Shi DL, Grifone R. RNA-binding proteins in the post-transcriptional control of skeletal muscle development, regeneration and disease. Front Cell Dev Biol 2021;9:. https://doi.org/10.3389/fcell.2021.738978738978.
[102] Frédérick PM, Simard MJ. Regulation and different functions of the animal microRNA-induced silencing complex. Wiley Interdiscip Rev RNA 2022;13 (4). https://doi.org/10.1002/wrna.1701.
[103] Schwanhäusser B et al. "Global quantification of mammalian gene expression control. Nature 2011;473(7347):337–42. https://doi.org/10.1038/nature10098.
[104] Hinnebusch AG, Ivanov IP, Sonenberg N. "Translational control by 5'-untranslated regions of eukaryotic mRNAs. Science 2016;352 (6292):1413–6. https://doi.org/10.1126/science.aad9868.
[105] Gage JL et al. Variation in upstream open reading frames contributes to allelic diversity in maize protein abundance. Proc Natl Acad Sci U S A 2022;119(14). https://doi.org/10.1073/pnas.2112516119.
[106] Hinnebusch AG. Structural insights into the mechanism of scanning and start codon recognition in eukaryotic translation initiation. Trends Biochem Sci 2017;42(8):589–611. https://doi.org/10.1016/j.tibs.2017.03.004.
[107] Wu Q, Wright M, Gogol MM, Bradford WD, Zhang N, Bazzini AA. Translation of small downstream ORFs enhances translation of canonical main open reading frames. EMBO J 2020;39(17). https://doi.org/10.15252/embj.2020104763.
[108] Xing J, Liu H, Jiang W, Wang L. LncRNA-Encoded Peptide: Functions and Predicting Methods. Front Oncol 2020;10:. https://doi.org/10.3389/fonc.2020.622294622294.
[109] Wang J, Zhu S, Meng N, He Y, Lu R, Yan GR. ncRNA-encoded peptides or proteins and cancer. Mol Ther 2019;27(10):1718–25. https://doi.org/10.1016/j.ymthe.2019.09.001.
[110] Wang S, Mao C, Liu S. "Peptides encoded by noncoding genes: challenges and perspectives. Signal Transduct Target Ther 2019;4:57. https://doi.org/10.1038/s41392-019-0092-3.
[111] Guerra-Almeida D, Tschoeke DA, Nunes-da-Fonseca R, Understanding small ORF diversity through a comprehensive transcription feature classification, DNA Res, vol. 28, no. 5, 2021, doi: 10.1093/dnares/dsab007.
[112] Mudge JM et al. Standardized annotation of translated open reading frames. Nat Biotechnol 2022. https://doi.org/10.1038/s41587-022-01369-0.
[113] Stellato C. "Post-transcriptional and nongenomic effects of glucocorticoids. Proc Am Thorac Soc 2004;1(3):255–63. https://doi.org/10.1513/pats.200402-015MS.
[114] Ishmael FT et al. "Role of the RNA-binding protein tristetraprolin in glucocorticoid-mediated gene regulation. J Immunol 2008;180 (12):8342–53. https://doi.org/10.4049/jimmunol.180.12.8342.
[115] Park OH, Do E, Kim YK. "A new function of glucocorticoid receptor: regulation of mRNA stability. BMB Rep 2015;48(7):367–8. https://doi.org/10.5483/bmbrep.2015.48.7.131.
[116] Miyake Y et al. "C-type lectin MCL is an FcRγ-coupled receptor that mediates the adjuvanticity of mycobacterial cord factor. Immunity 2013;38 (5):1050–62. https://doi.org/10.1016/j.immuni.2013.03.010.
[117] Chen ST et al. CLEC5A is a critical receptor in innate immunity against Listeria infection. Nat Commun 2017;8(1):299. https://doi.org/10.1038/s41467-017-00356-3.
[118] Greulich F, Bielefeld KA, Scheundel R, Mechtidou A, Strickland B, Uhlenhaut NH, Enhancer RNA Expression in Response to Glucocorticoid Treatment in Murine Macrophages, *Cells*, vol. 11, no. 1, 2021, doi: 10.3390/cells11010028.
[119] Greulich F, Wierer M, Mechtidou A, Gonzalez-Garcia O, Uhlenhaut NH. The glucocorticoid receptor recruits the COMPASS complex to regulate inflammatory transcription at macrophage enhancers. Cell Rep 2021;34(6). https://doi.org/10.1016/j.celrep.2021.108742.
[120] Escoter-Torres L, Greulich F, Quagliarini F, Wierer M, Uhlenhaut NH. Anti-inflammatory functions of the glucocorticoid receptor require DNA binding. Nucl Acids Res 2020;48(15):8393–407. https://doi.org/10.1093/nar/gkaa565.
[121] Syed AP, Greulich F, Ansari SA, Uhlenhaut NH, Anti-inflammatory glucocorticoid action: genomic insights and emerging concepts, Curr Opin Pharmacol, vol. 53, pp. 35-44, 08 2020, doi: 10.1016/j.coph.2020.03.003.
[122] Escoter-Torres L, Caratti G, Mechtidou A, Tuckermann J, Uhlenhaut NH, Vettorazzi S. Fighting the fire: mechanisms of inflammatory gene regulation by the glucocorticoid receptor. Front Immunol 2019;10:1859. https://doi.org/10.3389/fimmu.2019.01859.
[123] Uhlenhaut NH et al. Insights into negative regulation by the glucocorticoid receptor from genome-wide profiling of inflammatory cistromes. Mol Cell 2013;49(1):158–71. https://doi.org/10.1016/j.molcel.2012.10.013.